Western University
Scholarship@Western

Anatomy and Cell Biology Publications | Anatomy and Cell Biology Department

Spring 3-1-2014

Skin disease and non-syndromic hearing loss-linked Cx30 mutations exhibit several distinct cellular pathologies

Amy Berger
amy.berger@schulich.uwo.ca

John Kelly
john.kelly@schulich.uwo.ca

Patrick Lajoie
plajoie3@uwo.ca

Qing Shao
Cindy.shao@schulich.uwo.ca

Dale Laird
dwlaird@uwo.ca

Follow this and additional works at: https://ir.lib.uwo.ca/anatomypub

 Part of the Anatomy Commons, and the Cell and Developmental Biology Commons

Citation of this paper:

Berger, Amy; Kelly, John; Lajoie, Patrick; Shao, Qing; and Laird, Dale, "Skin disease and non-syndromic hearing loss-linked Cx30 mutations exhibit several distinct cellular pathologies" (2014). *Anatomy and Cell Biology Publications*. 8.
https://ir.lib.uwo.ca/anatomypub/8

Skin disease and non-syndromic hearing loss-linked Cx30 mutations exhibit several distinct cellular pathologies

Amy C. Berger[1]*, John J. Kelly[2]*, Patrick Lajoie[2], Qing Shao[2] and Dale W. Laird[1,2]

Departments of [1]Physiology and Pharmacology and [2]Anatomy and Cell Biology, University of Western Ontario, London, Ontario, Canada, N6A 5C1

* these authors contributed equally to this work and should be considered as joint first authors

Address Correspondence to:
Dale W. Laird, Ph.D.
Professor
Canada Research Chair in Gap Junctions and Disease
Department of Anatomy and Cell Biology
University of Western Ontario
Dental Science Building, Rm 00077
London, Ontario, Canada, N6A-5C1
Tel: (519) 661-2111 x86827
Fax: (519) 850-2562
Dale.Laird@schulich.uwo.ca

Running Title: Connexin30 mutations linked to disease

Keywords: Connexin, Gap junction, Hemichannel, Hearing loss, Skin disease, Mutation, Vohwinkel syndrome, Bart-Pumphrey syndrome, Clouston syndrome, Keratitis-ichthyosis-deafness syndrome

SUMMARY

Connexin 30 (Cx30), a member of the large gap junction protein family, plays a role in the homeostasis of the epidermis and inner ear through gap junctional intercellular communication (GJIC). Here, we investigated the underlying mechanisms of four autosomal dominant Cx30 gene mutations linked to hearing loss and/or various skin diseases. First, the T5M mutant linked to non-syndromic hearing loss formed functional gap junction channels and hemichannels, similar to wild type Cx30. The loss-of-function V37E mutant associated with Clouston syndrome or keratitis-ichthyosis-deafness syndrome was retained in the endoplasmic reticulum and significantly induced apoptosis. The G59R mutant linked to Vohwinkel and Bart-Pumphrey syndromes was retained primarily in the Golgi apparatus and exhibited loss of gap junction channel and hemichannel function, but did not cause cell death. Lastly, the A88V mutant related to Clouston syndrome also significantly induced apoptosis, although through an endoplasmic reticulum-independent mechanism. Collectively, we discovered that four unique Cx30 mutants may cause disease through different mechanisms that also likely include their selective transdominant effects on co-expressed connexins, highlighting the overall complexity of connexin-linked diseases and the importance of GJIC in disease prevention.

INTRODUCTION

Gap junctions are clusters of specialized intercellular channels that regulate the direct exchange of ions and various hydrophilic cellular metabolites smaller than 1000 Da, a process known as gap junctional intercellular communication (GJIC) (Alexander and Goldberg, 2003). Two inter-docked connexons (hemichannels), one from each of two apposing cells, form a functional gap junction channel. Each connexon is composed of six oligomerized connexin (Cx) subunits, and to date, the connexin family consists of 21 members in humans (Sohl and Willecke, 2003; Sohl and Willecke, 2004). Interestingly, while the primary function of gap junction channels is to facilitate intercellular communication, hemichannels have also been reported to exist and function at the cell surface in an undocked state, permitting the transfer of molecules between extracellular and intracellular environments (Anselmi et al., 2008; Burra and Jiang, 2011; Tong et al., 2007). Hemichannels formed from single or multiple types of connexins are termed homomeric and heteromeric, respectively, and gap junction channels are characterized as homotypic or heterotypic according to whether their channels are composed of the same or different connexons (Burra and Jiang, 2011). Channel composition depends on the connexin expression profile of each cell and tissue type, as well as the natural compatibility of the connexins to intermix (Beyer et al., 2013; Burra and Jiang, 2011; Laird, 2006).

Connexins are highly expressed in virtually all tissues in the human body, and GJIC plays an essential role in the regulation of cellular and physiological processes including proliferation, differentiation, apoptosis, growth and development (Alexander and Goldberg, 2003; Choudhry et al., 1997; Decrock et al., 2009; Kumar and Gilula, 1996; McLachlan et al., 2007). In the inner ear and the skin, proper connexin expression and function directly relate to the maintenance of cochlear homeostasis and epidermal differentiation, respectively (Langlois et al., 2007; Wangemann, 2006; Zhao et al., 2006). In the cochlea, Cx26, Cx29, Cx30, Cx31 and Cx43, found in the epithelial and connective tissue gap junction networks, play a crucial role in sound transduction. Cx26, and possibly other connexins, are thought to be involved in the recycling of K^+ through the supporting cells back to the endolymphatic space, for potential re-entry into sensory cells when activated by an acoustic stimulus (Kikuchi et al., 2000; Nickel and Forge, 2008). Interestingly, at least seven connexins, including Cx26, Cx30 and Cx43, are temporally and spatially expressed at the protein level in the human epidermis with overlapping distribution in the various non-cornified epidermal strata (Di et al., 2001; Kretz et al., 2004). While GJIC

plays an important role in epidermal differentiation, it is also critical to the wound healing process (Churko and Laird, 2013; Langlois et al., 2007). Here we focus on Cx30, which in humans, is predominantly expressed in the inner ear and epidermis (Di et al., 2001; Nickel and Forge, 2008).

Connexin mutations have been linked to a number of different diseases ranging from developmental disorders to congenital cataracts (Laird, 2006). Mutations in the genes encoding Cx26, Cx30, Cx30.3 and Cx31 in particular have been linked predominantly to hearing loss and various skin diseases (Di et al., 2001). Importantly, mutations in Cx30 and Cx26, the most predominant connexins in the inner ear (Hoang Dinh et al., 2009), are the leading cause of nearly half the cases of inherited prelingual non-syndromic hearing loss (Bitner-Glindzicz, 2002; Chang et al., 2009; Schutz et al., 2010; Wang et al., 2011). In particular, seven distinct single amino acid substitutions in the 1st half of the coding sequence of Cx30 are responsible for hearing loss and/or skin disease. The T5M (threonine to methionine at position 5) and A40V (alanine to valine at position 40) mutations have been linked to non-syndromic hearing loss as no other tissues or organs where Cx30 is expressed were affected (Grifa et al., 1999; Wang et al., 2011). Interestingly, hidrotic ectodermal dysplasia, commonly known as Clouston syndrome, is a skin disease distinctly linked to G11R (glycine to arginine at position 11) (Chen et al., 2010; Common et al., 2002; Zhang et al., 2003), V37E (valine to glutamic acid at position 37) (Common et al., 2002; Jan et al., 2004; Smith et al., 2002), D50N (aspartic acid to asparagine at position 50) (Baris et al., 2008) and A88V (alanine to valine at position 88) (Common et al., 2002; Essenfelder et al., 2004) Cx30 mutations. This rare disease has a founder effect within the French-Canadian population and is characterized by palmoplantar hyperkeratosis (PPK), nail dystrophies, and partial to complete alopecia (Kibar et al., 2000; Zhang et al., 2003). In some patients, other symptoms like ocular and craniofacial abnormalities, hearing loss and abnormal sweating and cardiac findings have been reported (Christianson and Fourie, 1996; Fraser and Der Kaloustian, 2001; Lamartine et al., 2000). Interestingly, one patient harbouring a V37E Cx30 mutation was diagnosed with keratitis-ichthyosis-deafness (KID) syndrome commonly associated with Cx26 mutations. This patient experienced Clouston syndrome-like symptoms, but also hearing impairment and vascularising keratitis (Jan et al., 2004). Finally, a G59R mutation results in the development of classical Vohwinkel syndrome and Bart-Pumphrey syndrome (Nemoto-Hasebe et al., 2009), which are also diseases most commonly caused by

mutations in Cx26 (Bakirtzis et al., 2003; Jan et al., 2004; Richard et al., 2004). Both syndromes result in PPK and sensorineural hearing loss, however, Bart-Pumphrey syndrome can be distinguished by the formation of knuckle pads, while patients with Vohwinkel syndrome develop constriction bands that cause spontaneous auto-amputation of the digits (pseudoainhum) (Bakirtzis et al., 2003; Richard et al., 2004).

Previously, studies on a few of the Cx30 disease-linked mutations have revealed reduced or abolished gap junction function, as the majority of mutant proteins are retained in subcellular compartments (Common et al., 2002; Essenfelder et al., 2004; Wang et al., 2011). Typically, most connexins follow the traditional secretory pathway by folding in the endoplasmic reticulum (ER), oligomerizing into connexons either in the ER or Golgi apparatus and by employing microtubules for efficient trafficking to the plasma membrane (Koval, 2006; Laird, 2006). Disruptions to any stage of this connexin transport process can have detrimental cellular effects and commonly results in connexin-linked disease (Laird, 2006).

Connexin mutations can lead to trafficking defects and their retention within the cell. In particular, intracellular accumulation of Cx50 and Cx31 mutants cause cell death associated with activation of ER stress signaling pathways (Alapure et al., 2012; Tattersall et al., 2009). Aberrant accumulation of misfolded secretory proteins in the ER triggers a process known as the unfolded protein response (UPR) (Malhotra and Kaufman, 2007). Typically, quality control mechanisms involving chaperones in the ER facilitate the re-folding of misfolded proteins for export out of the ER (Groenendyk and Michalak, 2005). The UPR involves the activation of three ER membrane-bound sensors (PERK, IRE1 and ATF6) that work collectively to attenuate protein translation, increase the folding capacity of the ER through the up-regulation of chaperone proteins, increase lipid synthesis and force misfolded proteins through an ER-associated degradation pathway to relieve ER stress and maintain cellular homeostasis (Malhotra and Kaufman, 2007). Failure of these processes to reduce ER stress results in the induction of apoptosis (Groenendyk and Michalak, 2005; Rasheva and Domingos, 2009).

Currently, it is poorly understood how Cx30 mutations manifest into syndromic and non-syndromic diseases involving the skin and cochlea. In the present study, we characterized four different Cx30 mutants, linked to non-syndromic hearing loss, Clouston syndrome, KID syndrome and Vohwinkel/Bart-Pumphrey syndromes to gain critical insight into the mechanisms behind these distinct disease manifestations. Our results indicate that the T5M mutant associated

with non-syndromic hearing loss formed functional gap junction channels, while the skin disease-linked mutants were primarily retained in intracellular compartments, reducing channel function. In addition, since we showed that Clouston syndrome-linked mutants induced cell death in keratinocytes, we investigated the potential mechanisms that cause cell death. Surprisingly, the ER-localized V37E mutant, did not substantially and consistently increase the expression of classical UPR markers, as would be predicted for misfolded proteins accumulating in the ER. However, V37E along with A88V mutant, activated a caspase-3 cleavage pathway to induce apoptosis. Finally, we demonstrated that skin disease-linked mutants are not rescued by co-expressed wild-type (wt) Cx30 or Cx26 in rat epidermal keratinocytes (REKs), and in particular, mutants associated with Clouston syndrome exhibit dominant-negative properties on these co-expressed connexins. Collectively, these studies demonstrate the complexity of the mechanisms involved in connexin-linked diseases, as one Cx30 mutant even exhibited intercellular channel and hemichannel function, yet still causes disease.

RESULTS

Cx30 mutations linked to skin disease and non-syndromic hearing loss, and their differential ectopic expression and localization in REKs – Cx30 is a 261 amino acid gap junction protein that exhibits the topological structure of a typical connexin, with four transmembrane domains, two extracellular loops, one intracellular loop and cytoplasmic-exposed amino and carboxy termini (Fig. 1A). The location of four distinct mutations that cause skin disease and/or hearing loss are all located within the 1st half of the Cx30 protein (Fig. 1A).

Western blot analysis was used to determine the expression levels of green fluorescent protein (GFP)-tagged T5M, V37E, G59R and A88V mutants in REKs. Quantification of densitometry values revealed that V37E-GFP and A88V-GFP protein levels were ~35% and ~50% lower, respectively, compared to the relative expression of Cx30-GFP (**P<0.01) (Fig. 1B, C). In contrast, the non-syndromic hearing loss-linked T5M and Vohwinkel syndrome-linked G59R mutants exhibited expression levels similar to that of Cx30-GFP.

To compare the localization profiles of the mutant forms of Cx30, we examined GFP-tagged Cx30 mutants (Fig. 2A) and untagged Cx30 mutants (Fig. 2B, C) in REKs. Consistent with previous reports, the T5M mutant formed gap junction-like plaques at the cell surface similar to wt Cx30, while the V37E and A88V Clouston syndrome-linked mutants appeared to

remain in intracellular compartments (Common et al., 2002; Essenfelder et al., 2004) (Fig. 2A, B). Immunolabeling for the ER-resident protein disulfide isomerase (PDI) revealed that the Clouston syndrome/KID syndrome-linked V37E mutant was retained in the ER (Fig. 2A). A88V mutant-expressing cells appeared to be entering a cell death pathway as they exhibited small and fragmented nuclei, and since they lacked PDI staining, it remains unclear whether a significant population of this mutant resides in the ER. The novel Vohwinkel syndrome-linked G59R mutant (Nemoto-Hasebe et al., 2009) also showed an intracellular localization profile (Fig. 2A, B), and immunolabeling for Golgi matrix protein 130 (GM130) revealed its localization largely in the Golgi apparatus (Fig. 2C). Interestingly, while we have never observed V37E plaques at the interface between apposing cells, a population of the G59R and A88V mutants successfully trafficked to the cell surface to form gap-junction-like plaques (Fig. 2A, B, arrows). Cx30 and Cx30 mutants all similarly localized within the cell regardless of the presence or absence of the GFP tag (Fig. 2A-C).

V37E and A88V Cx30 mutants affect endogenous Cx43 localization in REKs and ectopic Cx43 localization in HeLa cells – To determine whether the presence of the Cx30 mutants affected endogenous Cx43 localization, REKs were engineered to express Cx30-GFP or the equivalent GFP-tagged mutants. For the T5M and G59R mutants, Cx43 frequently co-localized with Cx30 mutants at cell-cell interfaces, whereas Cx43-based gap junctions appeared less frequently between cells expressing the V37E and A88V mutants (Fig. 3A). The total protein levels of Cx43, however, remained unchanged (Fig. 3B, C). Total Cx43 levels were only slightly decreased in T5M mutant-expressing cells compared to those expressing Cx30 ($*P<0.05$). In agreement with these findings, HeLa cells that were engineered to express Cx30 mutants with Cx43-RFP showed similar localization profiles (Fig. S1). Both wt Cx30 and T5M frequently co-localized in plaque-like structures, whereas cells expressing V37E and A88V mutants exhibited less plaque formation and Cx43 was more evident in intracellular compartments. The G59R mutant had reduced plaque-like structures but it did not prevent Cx43 from trafficking to the cell surface (Fig. S1).

V37E and G59R skin disease-linked Cx30 mutants exhibit loss of gap junction function in HeLa cells – Since the T5M mutant and a population of the G59R mutant formed

punctate gap junction-like structures at the cell surface in REKs, we hypothesized that these mutants may form functional gap junctions. Mutant-expressing GJIC-deficient HeLa cells were microinjected with Alexa 350 to assess whether any of the mutants restored GJIC. As expected, Cx30 gap junction channels readily facilitated dye transfer (***P<0.001), while untransfected (Untr) and free GFP-expressing cells showed no significant dye transfer to surrounding cells (Fig. 4A, B). Interestingly, the T5M mutant exhibited dye transfer in ~90% (***P<0.001) of cells injected (Fig. 4A, B), indicating that this mutant was functional. No dye transfer was observed in microinjected HeLa cells expressing the V37E and G59R mutants (Fig. 4A, B). A88V-expressing cells were not included in these functional studies, as they could not be microinjected due to their porous cell membranes caused by cell death (see Fig. 5C).

V37E and A88V Cx30 mutants reduce coupling in Cx43-positive REKs – Since the Cx30 mutants had the ability to affect Cx43 localization, we wanted to determine whether Cx30 mutants affected GJIC in Cx43-rich REKs. GFP-tagged mutant-expressing REKs were microinjected with Alexa 350 in a region where cell clusters were expressing GFP, and the incidence of dye transfer was recorded. Untransfected REKs exhibited 100% dye transfer, and no significant differences in dye transfer were observed in REKs expressing GFP, Cx30, or the T5M and G59R mutants (Fig. 4C, D). In contrast, cell pairs or clusters expressing the V37E and A88V mutants exhibited significantly decreased Cx43-mediated dye transfer (**P<0.01) (Fig. 4C, D).

The V37E and G59R mutants do not form functional cell surface hemichannels – The ability of each Cx30 mutant to form functional hemichannels was investigated by observing the incidence of propidium iodide (PI) dye uptake in Cx30 or mutant expressing HeLa cells under normal extracellular solution (ECS) and Ca^{2+}/Mg^{2+} divalent cation free ECS (DCF-ECS) conditions, which induces hemichannels to open (Lai et al., 2006; Stout et al., 2002). Under ECS conditions, any putative Cx30, T5M, V37E or G59R mutant hemichannels would remain closed and as expected, no dye uptake was observed (Fig. 5A). Under DCF-ECS conditions, ~90% of isolated T5M-expressing cells exhibited dye uptake, closely resembling the ~95% incidence observed for cells expressing Cx30, both of which were significantly higher than that observed under control ECS conditions (***P<0.001) (Fig. 5A, B). In contrast, the V37E and G59R

mutant expressing cells did not exhibit any dye uptake in DCF-ECS conditions. The loss of cell membrane integrity was evident in A88V mutant expressing cells since ~75% of the cells exhibited uptake of the hemichannel impermeable dye dextran-rhodamine (MW, 10 kDa) in normal ECS conditions. In contrast, wt Cx30 expressing cells did not uptake dextran-rhodamine in ECS (Fig. 5C). Collectively, these studies indicated that V37E and G59R mutants were loss-of-function mutants while the T5M mutant showed similar functional channel properties to Cx30. The A88V mutant caused membrane disruption and cell death 24 hours after expression, therefore hemichannel status could not be assessed.

V37E and A88V mutants induce apoptosis by distinct mechanisms – The ectopic expression of the V37E and A88V mutants induced some degree of cell death in REKs as early as 18 hours post-expression, with the majority of A88V-expressing cells dying within 48 hours (data not shown). To determine the mechanism of cell death induced by these mutants, control and mutant-expressing REKs were immunolabeled with anti-cleaved caspase-3, a marker of the committed stage of apoptosis (Saraste and Pulkki, 2000). Interestingly, some V37E- and A88V-expressing REKs expressed cleaved caspase-3, indicating that these cells were undergoing apoptosis (Fig. S2). To further validate and quantify this finding, TUNEL assays representing the degradation stage of apoptosis (Saraste and Pulkki, 2000) were performed on Cx30- and mutant-expressing REKs. V37E and A88V Cx30 mutants significantly induced apoptosis, as ~70% and ~80% of GFP-expressing cells, respectively, were ApopTag positive (***P<0.001) compared to GFP only REKs, of which only ~2% were ApopTag positive (Fig. 6A, B). Untr cells treated with staurosporine (Stauro) for 24 hours served as a positive control for the assay, as ~90% of total cells were apoptotic in comparison to Untr controls (***P<0.001, Fig. 6C).

Since some of the mutants localized to the ER we wanted to determine whether apoptosis was triggered by an ER stress-mediated unfolded protein response (UPR). Western blot analyses of REK cell lysates were performed to detect changes in levels of markers involved in different stages and pathways of the UPR. REKs treated with tunicamycin (Tm), an ER stress inducer that blocks N-glycosylation of proteins (de Freitas Junior et al., 2011), served as positive controls for UPR markers. When compared to GFP-expressing cells, GRP78 expression was not elevated in any mutant-expressing cells (Fig. S3A). The activating transcription factor 4 (ATF4) was mildly up-regulated in cells expressing only the V37E mutant (***P<0.001) (Fig. S3B). Finally, the

C/EBP homologous protein (CHOP) was not elevated in any mutant expressing cells when compared to GFP expressing control cells and only significantly increased in tunicamycin (Tm)-treated cells (Fig. S3C).

To determine whether the Cx30 V37E mutant activates the IRE1 arm of the UPR we performed an X-box binding protein 1 (XBP1) splicing assay (Calfon et al., 2002; Williams and Lipkin, 2006). In response to unfolded proteins, IRE1 directly splices a small intron from XBP1 mRNA (Ron and Walter, 2007) containing a single *Pst*I restriction site (Fig. S3D-G). Agarose gel analysis of XBP1 cDNA confirmed the presence of the unspliced product in Untr controls as determined by the doublet band at ~300 bp (XBP1u) and low expression of the spliced 575 bp band (XBP1s) after *Pst*I digestion (Fig. S3F). The Tm control had elevated levels of undigested cDNA (575 bp) and a complete loss of the unspliced fragments (XBP1u), suggesting the vast majority of XBP1 mRNA was spliced. In comparison to the untransfected control, Cx30 and the T5M, V37E, G59R and A88V mutants displayed no discernible differences in XBP1 splicing (Fig. S3F). Detailed images of the higher bands (Fig. S3F) revealed a slight increase in XBP1s (575 bp) in comparison to XBP1u (601 bp) for transfected cells, but this was most likely a result of protein over-expression. The ratio of the 575 bp band to the ~300 bp doublet band showed that only the Tm control significantly induced splicing of XBP1 mRNA (Fig. S3G, N = 6, $***P<0.001$), suggesting that the V37E mutant did not induce an IRE1-mediated UPR.

V37E and A88V mutants may exhibit dominant-negative and transdominant effects on wt Cx30 and Cx26 when co-expressed in REKs – To determine whether skin disease-linked Cx30 mutants localized to intracellular compartments could be rescued to the cell surface, REKs were engineered to express red fluorescent protein (RFP)-tagged Cx30 (Cx30-RFP) or Cx26-RFP simultaneously with GFP-tagged Cx30 mutants. Alone, Cx30-RFP formed gap junctions (Fig. 7), which also facilitated the transfer of Alexa 350 in HeLa cells and REKs (data not shown). Cx30-GFP and T5M-GFP showed distinct co-localization with Cx30-RFP, with limited intracellular localization, whereas wt Cx30 did not appear to rescue the V37E mutant to the cell surface (Fig. 7). Although the G59R and A88V mutants showed some co-localization with wt Cx30 at the cell surface, the majority of these mutants were localized in intracellular compartments indicating that co-expression with wt Cx30 was not enough to fully rescue the trafficking of Cx30 mutants to the cell surface. (Fig. 7). Notably, the V37E and A88V mutants

may exhibit partial dominant-negative effects on wt Cx30, as a large population of Cx30-RFP was retained inside the cell as compared to situations where Cx30-RFP was expressed alone (Fig. 7). In particular, the A88V mutant and wt Cx30 exhibited overlapping co-localization in a distinct subcellular compartment. We also observed similar results in HeLa cells, whereby the V37E, G59R and A88V mutants all exhibited small amounts of co-localization with wt Cx30 at the cell surface, but the vast majority of mutant protein was localized intracellularly (Fig. S4). Alone, Cx26-RFP formed gap junctions in REKs (Fig. 8). Cx30-GFP, T5M-GFP and G59R-GFP also showed co-localization with Cx26-RFP, however the V37E, A88V and the majority of the G59R mutant remained within intracellular compartments indicating that wt Cx26 did not rescue the trafficking of these mutants (Fig. 8). However, the V37E and A88V mutants also may exhibit transdominant effects on Cx26, as the majority of Cx26-RFP was retained inside the cell compared to when Cx26-RFP was expressed alone (Fig. 8). Again, similar results were also obtained in HeLa cells engineered to express Cx30 and Cx30 mutants with Cx26-RFP. Cx30 and T5M showed strong co-localization at gap junction plaques (Fig. S4). The G59R mutant also co-localized strongly with Cx26-RFP at gap junction plaques, but a population of the mutant remained within intracellular compartments. The V37E mutant appeared to have transdominant effects on Cx26-RFP by reducing the evidence of Cx26-RFP found in plaques, whereas a portion of A88V could traffic to the cell surface with Cx26-RFP (Fig. S4).

DISCUSSION

In the present study, we first determined that the T5M mutant linked to non-syndromic hearing loss exhibited similar properties to wt Cx30, as it formed functional gap junctions and hemichannels. Skin disease-linked mutants exhibited impaired gap junction formation and function. In particular, the V37E mutant linked to KID syndrome was retained in the ER and triggered apoptosis, leading to the hypothesis that this was occurring via the UPR. However, only the UPR marker ATF4 was modestly elevated in cells that expressed this mutant with all other indices of UPR remaining unchanged. This suggests that cell death was likely triggered by an UPR independent mechanism. In contrast, the G59R mutant associated with Vohwinkel and Bart-Pumphrey syndromes was primarily retained in the Golgi apparatus, and did not induce cell death. The A88V mutant linked to Clouston syndrome remained primarily in intracellular compartments, but did have the capability of reaching the cell surface. Nevertheless, it potently

induced apoptosis possibly through mechanisms that could include leaky hemichannels that may occur within an intracellular compartment or at the cell surface. Finally, we determined that skin disease-linked mutants retained in intracellular compartments were not effectively rescued to the cell surface by co-expressed Cx43, Cx30 or Cx26, and the V37E and A88V mutants exhibited dominant-negative and transdominant effects on the trafficking of these connexins to the cell surface. Thus, we clearly demonstrated the overall complexity of connexin-linked diseases, as each Cx30 mutant exhibited markedly different characteristics and transdominant properties within cells. These findings also show that the disease phenotype correlates with the severity of the mutant on cellular health and overall GJIC.

In order to evaluate the link between Cx30 mutants and disease, we used spontaneously immortalized, newborn REKs, which have previously been reported to express messenger RNA (mRNA) for 9 connexins, including Cx30 (Maher et al., 2005), and are phenotypically similar to basal keratinocytes given their ability to differentiate and stratify (Langlois et al., 2007; Maher et al., 2005; Thomas et al., 2007). At the protein level, REKs abundantly express Cx43, and only express Cx26 upon differentiation (Maher et al., 2005). The fact that REKs did not express detectable levels of Cx30 allowed us to express and track both GFP-tagged and untagged versions of Cx30 and mutants. Similar localization profiles and function were observed for all GFP-tagged and untagged Cx30 and Cx30 mutants, strongly suggesting that the presence of GFP on the C-terminal tail did not affect the properties of Cx30, similar to what has been reported for Cx26 (Marziano et al., 2003) and Cx43 (Jordan et al., 1999).

The non-syndromic hearing loss-linked T5M mutant. The T5M mutant is one of only two Cx30 mutants linked specifically to non-syndromic hearing loss (Grifa et al., 1999; Wang et al., 2011). Consistent with our results, the T5M mutant was previously found to form gap junctions (Common et al., 2002), however, its functional capacity remains controversial. *In vitro* electrophysiological studies previously showed that the T5M amino acid substitution drastically reduced electrical coupling between *Xenopus laevis* oocytes (Grifa et al., 1999), while other reports showed restrictions in the transjunctional molecules that can pass through T5M channels (Common et al., 2002; Schutz et al., 2010; Zhang et al., 2005). In our study, we found that both T5M-based hemichannels and gap junction channels were functional to the passage of sizable

molecules (e.g. prodium iodide, Alexa 350) in mammalian cells, raising the question as to why this mutant causes hearing loss.

The answer may be linked to subtle changes in the N-terminal domain of Cx30 where the 'threonine' to 'methionine' substitution occurs. Cx30 shares 76% sequence homology with Cx26 (Grifa et al., 1999), and while the crystal structure of Cx30 has not yet been resolved, the crystal structure of Cx26 has elucidated that the amino terminal tail lines the gap junction channel pore, creating a funnel that restricts channel selectivity based on molecular size, flexibility, charge and charge distribution (Harris, 2007; Kwon et al., 2011; Maeda et al., 2009). In the non-sensory cells of the inner ear, Cx26 and Cx30 intermix to form heteromeric and heterotypic channels (Ahmad et al., 2003; Forge et al., 2003; Marziano et al., 2003; Yum et al., 2007), and are suggested to form functional hemichannels (Gossman and Zhao, 2008; Zhao et al., 2005). Through extrapolation, a mutation of the highly conserved hydrophilic T5 Cx30 amino acid (Grifa et al., 1999) may alter the permeability properties of both homotypic Cx30 and heterotypic Cx26/Cx30 channels. Another possibility may be how the T5M mutant affects Cx26, since the role of Cx30 in hearing remains controversial (Boulay et al., 2013; Miwa et al., 2013; Teubner et al., 2003) and increasing evidence suggests that Cx26 and Cx30 are co-regulated (Boulay et al., 2013). Expression levels of Cx26 were dramatically reduced in Cx30 knock-out (Boulay et al., 2013) and in Cx30 T5M knock-in mice that also exhibited decreased levels of Cx30 (Schutz et al., 2010). Importantly, in the inner ear, this mutant may be affecting Cx26 levels, potentially reducing the frequency of heteromeric and heterotypic channel formation necessary for K^+ buffering. In addition, Cx30 has been reported to be involved in glucose uptake and metabolic coupling between mouse cochlear cells (Chang et al., 2008). Therefore, the T5M mutation, although able to pass ions and molecular dyes, may reduce, but not inhibit, the permeability of metabolites such as glucose between supporting cells in the avascular sensory epithelium. However further investigation is necessary to clearly understand how the T5M mutation has such effects.

Our finding that T5M gap junction channels and hemichannels are functional agrees in part with other findings that suggest ionic permeability is not affected by this amino acid substitution (Schutz et al., 2010; Zhang et al., 2005). However, larger molecules such as propidium iodide (PI) (Zhang et al., 2005), inositol trisphosphate (IP3) and calcein (Schutz et al., 2010) have been reported to have reduced permeability. The intercellular transfer of calcein and

IP3 was observed between cells obtained from organotypic cochlear cultures from $Cx30^{T5M/T5M}$ mice where Cx26 is also known to be co-expressed. Thus, the presumed heteromeric conformation of $Cx30^{T5M}$/Cx26 channels may have an overriding effect on channel permeability/selectivity in comparison to homomeric T5M channels. However, the ability for the T5M mutant to uptake PI and transfer Alexa 350 in our study contrasts to that by (Zhang et al., 2005) and (Common et al., 2002), respectively. We can only speculate on this issue and suggest it may be due to differences in linker sequences joining the T5M mutant to GFP or differences in species sequences. Nevertheless, the fact that the T5M mutant is functional has been rigorously established suggesting that disease is likely linked to more subtle changes in channel regulation or changes in the structure of the amino terminus.

The loss-of-function V37E mutant linked to Clouston and KID syndromes. Although previously considered to be linked distinctly to Clouston syndrome (Common et al., 2002; Smith et al., 2002), the V37E mutant has now also been implicated in KID syndrome (Jan et al., 2004). Other than the fact that the V37E mutant was retained in an unknown intracellular compartment (Common et al., 2002), little was known about this mutant. Here, we conclusively show that the V37E mutant is retained within the ER where it is surveyed by molecular machinery as part of cellular quality control (Kleizen and Braakman, 2004). Furthermore, this loss-of-gap junction channel and -hemichannel function mutant acted in a (trans)dominant-negative fashion on co-expressed Cx43, Cx26 and Cx30 and significantly induced apoptosis in REKs.

The V37E mutant is positioned in the 1st transmembrane domain of Cx30. According to the crystal structure of Cx26, the 1st transmembrane domain is the major pore-lining helix involved in prominent intra-connexin interactions with all other transmembrane domains, which stabilizes the basic structure of the connexin subunit (Maeda et al., 2009). In addition, the V37 amino acid is located in a motif (VVAA) conserved between Cx26 and Cx30 (Maeda et al., 2009; Smith et al., 2002), and as demonstrated by the V37I Cx26 mutant, mutations within this particular motif reduce hexamer formation and channel function (Jara et al., 2012). Importantly, the V37E Cx30 mutation involves a more unique and critical substitution of a hydrophobic 'valine' with an acidic 'glutamic acid' residue, which we propose alters critical intra-connexin interactions and Cx30 stability, resulting in improper folding and protein accumulation in the ER. In addition, various Cx26 mutants linked to Vohwinkel syndrome and PPK have been

reported to exhibit dominant-negative and transdominant effects on other connexins, including Cx30 and Cx43 (Forge et al., 2003; Marziano et al., 2003; Rouan et al., 2001). While V37E Cx30 may exhibit these effects on co-expressed wt Cx30, Cx26 and Cx43, it is also possible that V37E-mutant expressing cells undergoing apoptosis are internalizing these connexins, as has been reported for Cx43 (Kalvelyte et al., 2003).

When the V37E mutant was expressed in keratinocytes, it induced apoptotic cell death that we hypothesized might occur through the UPR. The UPR is a protective cellular mechanism regulated by luminal ER chaperone GRP78 (Malhotra and Kaufman, 2007), and is involved in normal keratinocyte differentiation (Sugiura et al., 2009) as well as normal lens development (Alapure et al., 2012). Of note, mutations in Cx31 and Cx50 linked to erythrokeratoderma variabilis (EKV) and cataracts, respectively, induce an abnormal ER stress-mediated UPR (Alapure et al., 2012; Tattersall et al., 2009) and result in extensive cell death (Di et al., 2002; He et al., 2005). While the expression of the V37E Cx30 mutant did not induce the up-regulation of GRP78, which may occur upon the activation of the activating transcription factor 6 (ATF6) pathway (Berridge, 2002), the V37E mutant only moderately induced the expression of ATF4. ATF4 activates cell death-initiating caspases, including caspase 3, through the mitochondrial-dependent intrinsic cell death pathway (Galehdar et al., 2010; Groenendyk and Michalak, 2005; Malhotra and Kaufman, 2007). In contrast, the ER-stress induced splicing of XBP1 via IRE1 was negative in V37E mutant expressing cells, suggesting that the mechanism of cell death may in fact be independent of the UPR. This was somewhat surprising since the V37E mutant clearly accumulates in the ER and initiates apoptosis. However, evidence exists which suggests that misfolded secretory proteins, such as an α_1-antitrypsin Z mutant, can accumulate in the ER, induce ER vesiculation and activate caspase-dependent pathways without activating the UPR (Hidvegi et al., 2005). In addition, NFκB activation and calcium release from the ER via an alternative ER overload response (EOR) pathway have also been demonstrated to be distinct from the UPR (Pahl et al., 1996). Various stresses such as changes in ER calcium (Subramanian and Meyer, 1997) can similarly alter ER structure but the functional relevance of these alterations is unclear. Whether the V37E mutant is causing cell death through these alternative UPR-independent pathways remains to be determined, but the short time frame and rapid activation of apoptosis makes further dissection of the mechanisms involved difficult to ascertain.

The loss-of-function G59R mutant linked to Vohwinkel/Bart-Pumphrey syndromes. Here, a previously uncharacterized loss-of-function Cx30 G59R mutant was found to occasionally form gap junction plaques, but was mainly localized to the Golgi apparatus. This is consistent with findings for Vohwinkel syndrome-linked G59A and D66H Cx26 mutants (Bakirtzis et al., 2003; Marziano et al., 2003; Thomas et al., 2004), suggesting that mutations in the 1st extracellular domain of Cx30 and Cx26 may lead to similar disease phenotypes. Supporting the essential role of the 1st extracellular loop, the N45K Cx26 mutation located in this domain causes Bart-Pumphrey syndrome (Richard et al., 2004). The evolutionarily conserved 1st extracellular loop of Cx26 (and by extension Cx30) has been suggested to play a role in voltage gating (Tang et al., 2009; Verselis et al., 2009), and more importantly, inter-connexin and inter-connexon interactions (Maeda et al., 2009). Therefore, the Cx30 G59R mutant may result in defective connexin oligomerization, which occurs primarily in the ER and Golgi apparatus for several connexins including Cx32, Cx26, Cx43 and Cx46 (Das Sarma et al., 2002; Evans et al., 1999; Koval et al., 1997; Musil and Goodenough, 1993). Reduced channel function at the cell surface may also indicate defective hemichannel docking, highlighting the importance of this domain in channel formation and function linked to hearing loss and skin diseases.

The A88V mutant linked to Clouston syndrome. The A88V mutant is one of four mutations linked to Clouston syndrome. Previous studies localized the A88V mutant to intracellular compartments, which could be partially rescued to the cell surface when co-expressed with wt Cx30 (Common et al., 2002; Essenfelder et al., 2004). The A88V mutant was also found to exhibit abnormal hemichannel activity associated with ATP release and subsequent cell death (Essenfelder et al., 2004). We extended these studies by demonstrating that a population of the A88V mutant also formed gap junction-like structures, and negatively affected Cx43-based gap junction coupling and the trafficking of both wt Cx26 and Cx30. These dominant-negative and transdominant effects may also be cumulated with the fact that the A88V mutant significantly induced apoptosis in REKs, similar to our suggestion for the V37E mutant.

Clearly, the A88 amino acid is critical for Cx30 hemichannel and channel function. Cx30 forms voltage-gated hemichannels (Valiunas and Weingart, 2000), which are normally closed under physiological conditions and open in response to low extracellular concentrations of Ca^{2+} and Mg^{2+} (De Vuyst et al., 2007; Tong et al., 2007; Verselis and Srinivas, 2008). Importantly,

leaky hemichannels resulting in cell death have been reported for a number of other connexin mutations (Gerido et al., 2007; Lee et al., 2009; Mese et al., 2011; Stong et al., 2006), and also for the A88V Cx26 mutation which is linked to KID syndrome (Mhaske et al., 2013). The crystal structure of Cx26 suggests that part of the 2nd transmembrane domain also lines the channel pore and is involved in intra-connexin interactions with other domains including the amino terminus that dictate specific protein conformation (Kwon et al., 2011; Maeda et al., 2009). By analogy, it is possible that the A88V Cx30 mutation affects protein folding and stability, and alters important interactions, moving the amino terminal domain away from the cytoplasmic entrance of the pore (Kwon et al., 2011; Maeda et al., 2009) to favour abnormal hemichannel activity. Therefore, we propose that leaky A88V Cx30 hemichannels contribute to induced apoptosis in REKs. Since Cx30 likely oligomerizes early in the secretory pathway, leaky A88V hemichannels (or connexons) would disrupt the calcium gradient in the ER and other compartments possibly triggering a rapid cell death response.

In conclusion, the present study characterized four Cx30 mutations linked to skin disease (A88V), hearing loss (T5M) and combinations of both (V37E and G59R). Each mutation results in disease manifestations through distinct mechanisms ranging from a mutant that exhibits wild type Cx30 characteristics (T5M) to mutants that induce apoptosis through possible constitutive and premature activation of hemichannels, or through ER signalling mechanisms that are UPR-independent (A88V, V37E). Moreover, the loss-of-function G59R mutant causes yet another skin disease phenotype manifesting as a combination of Vohwinkel and Bart-Pumphrey syndromes. While all of these Cx30 autosomal dominant gene mutations cause syndromic and non-syndromic disease by different mechanisms, future studies will need to determine the key role of co-regulated connexins in the cochlea and epidermis.

MATERIALS AND METHODS

Generation of cDNA constructs

Mouse Cx30 complementary DNA (cDNA) encoded within the pBluescript vector, kindly provided by Dr. C. C. Naus (UBC, Vancouver, BC), was cloned into a pEGFP expression vector using XhoI and NotI restriction enzymes. This combination of restriction enzymes removes the enhanced GFP (eGFP) cDNA from the vector as described by Thomas et al. (2004). Cx30 mutants were constructed using the QuikChange site-directed mutagenesis kit (Stratagene,

La Jolla, CA) as per the manufacturer's instructions. The following primer pairs were used to create the Cx30 mutations. The nucleotide change is underlined in each case:

T5M: sense, 5'-GCACGATGGACTGGGGGATGCTGCACACCGTCATCGG-3'; antisense, 5'-CCGATGACGGTGTGCAGCATCCCCCAGTCCATCGTGC-3';

V37E: sense, 5'-CCGAGTCATGATCCTAGAGGTGGCTGCCCAG-3'; antisense, 5'-CTGGGCAGCCACCTCTAGGATCATGACTCGG-3';

A88V: sense, 5'-CTTTGTGTCTACCCCAGTCCTGTTGGTGGCCATGC-3'; antisense, 5'-GCATGGCCACCAACAGGACTGGGGTAGACACAAAG-3'.

The G59R mutant was purchased from Norclone Biotech Laboratories (London, ON). All mutations were validated by sequencing, indicating the presence of the mutation and ensuring that no other mutations were introduced.

To create GFP-tagged constructs and Cx30-RFP, polymerase chain reaction (PCR) was performed to introduce XhoI and EcoRI restriction sites to the 5' and 3' ends of the Cx30 and Cx30 mutant sequences; respectively, removing the stop codon and allowing for the expression of GFP. Following digestion with XhoI and EcoRI restriction enzymes, the PCR products were cloned into the pEGFP-N1 (Clontech, Palo Alto, CA) and pTagRFP-N (Evrogen, Cedarlane as distributor, Burlington, ON) vectors to produce GFP-tagged constructs and Cx30-RFP, respectively. Cx43-mRFP was kindly provided by Dr. Guido Gaietta (University of California, San Diego, CA) as described before (Gong et al., 2007). For Cx26-RFP, Cx26 cDNA was digested from Cx26-YFP (Laird et al., 2001) by using XhoI and EcoRI restriction enzymes and directly subcloned into pTagRFP-N vector as mentioned above. All constructs were sequenced for verification.

Cell Culture and Transient Transfections

GJIC-competent REKs, kindly provided by Dr. Vincent C. Hascall (Cleveland Clinic, Cleveland, OH), and communication-deficient HeLa cells (ATCC, Manassas, VA) were cultured in high glucose Dulbecco's modified Eagle's medium (DMEM) supplemented with 10% fetal bovine serum, 100 U/mL penicillin, 100 µg/mL streptomycin and 2 mM L-glutamine (Invitrogen, Burlington, ON), in a humidified incubator maintained at 37°C with 5% CO_2 as previously described (Maher et al., 2005). Cells were passed once they reached 80-100% confluency using 0.25% trypsin-ethylenediaminetetraacetic acid (trypsin-EDTA) (Invitrogen),

and were cultured in 35 mm or 60 mm plastic tissue culture dishes for all experimental procedures. Prior to transfection, all cells were grown to 65-80% confluency, and those destined for immunolabeling or terminal deoxynucleotidyl transferase dUTP nick end labelling (TUNEL) assays were also grown on glass coverslips. Cells were transfected with 2-6 µg of DNA using Lipofectamine 2000 (Invitrogen) in the presence of low serum OptiMEM medium (Invitrogen) as previously described (Penuela et al., 2007) or using the JetPRIME-mediated transfection kit (VWR International, Mississauga, ON) according to the manufacturer's instructions. As controls, untransfected cells were exposed to transfection reagents and the appropriate media without the addition of any DNA. As a second control, a population of cells was also transfected with a vector encoding free GFP. Co-transfections were performed using the Polyplus JetPRIME transfection method by mixing 1µg of Cx30- or Cx26-RFP and 1 µg of each GFP-tagged Cx30 mutant. All transfections were terminated after 24 hours. Positive controls for the induction of ER stress or apoptosis included cells plated in parallel, treated for 24 hours with 2 µg/mL tunicamycin or 0.5 µg/mL staurosporine, respectively (both from Sigma Aldrich, St Louis, MO).

Immunocytochemistry

Cells grown in monolayer on glass coverslips were fixed with 10% neutral buffered formalin (NBF) (EMD Millipore, Billerica, MA) for 25 minutes at room temperature. In a humidified chamber, fixed cells were blocked for 30-45 minutes at room temperature in phosphate buffered saline (PBS) containing 2% bovine serum albumin (BSA) (Santa Cruz Biotechnology, Dallas, TX), to prevent non-specific antibody binding, and 0.1% Triton X-100 (Sigma Aldrich) for permeabilization. Endogenous or ectopic connexin expression and localization was detected by labeling with rabbit anti-Cx43 (1:500, Sigma Aldrich) or anti-Cx30 (1:500, Invitrogen) antibodies for 1 hour. In some cases, cells were labeled with mouse anti-PDI (1:500, Enzo Life Sciences, Farmingdale, NY) to denote the position of the ER, mouse anti-GM130 (1:500, BD Transduction Laboratories, Mississauga, ON) to demarcate the Golgi apparatus or rabbit anti-cleaved caspase-3 (1:1000, Cell Signaling Technology, Danvers, MA) to denote cells undergoing apoptosis. Cells were then incubated with secondary AlexaFluor555 or AlexaFluor488 conjugated antibodies (1:500, Invitrogen) for 45-60 minutes, and stained for 5-10 minutes with Hoescht 33342 (1:1000, Invitrogen) to denote the nuclei. Cells were mounted on

glass microscope slides. Cells co-transfected with Cx30- or Cx26-RFP and GFP-tagged Cx30 mutants were not immunolabeled, but were stained with Hoescht 33342 and mounted as described above. All slides were stored at 4°C with minimal exposure to light. Slides were imaged using a Zeiss LSM 510 confocal microscope (Thornwood, NY) equipped with a 63X lens as previously outlined by Thomas et al. (2007).

Microinjection Assays

In order to test Cx30 and mutant gap junction function, REKs and HeLa cells ectopically expressing Cx30 or mutants were microinjected with 10 mM Alexa Fluor 350 hydrazide (Invitrogen) using an automated Eppendorf FemtoJet microinjection system (Mississauga, ON) as previously described (Huang et al., 2013). For each biological replicate of GFP-, Cx30-, T5M-, V37E- and G59R-expressing cells, ~15-20 cells were microinjected and the incidence of dye transfer to surrounding cells was recorded. Images were acquired using a Leica DM IRE2 inverted epifluorescent microscope (Richmond Hill, ON), equipped with a Hamamatsu digital camera (Bridgewater, NJ) and OpenLab 5.5.3 Imaging Software (Lexington, MA). HeLa cells expressing the A88V mutant could not be microinjected due to the fact that cells were already undergoing cell death and had a permeable cell membrane, however in the case of REKs, 5-10 cells were microinjected in each replicate. REKs and HeLa cells were microinjected and processed in the same manner to ensure that cells were well coupled and connexin-deficient, respectively. A one-way ANOVA was performed on the averages of 3 biological replicates, and values represent the mean percent incidence of dye transfer ± s.e.m.

Dye Uptake Hemichannel Assays

To assess Cx30 and mutant hemichannel function, dye uptake assays were performed as previously described by Tong et al. (2007) with some modifications. Briefly, HeLa cells plated as single isolated cells were transfected with 1.5 µg of DNA as described above using Lipofectamine 2000. Normal extracellular solution (ECS, in mM: 142 NaCl, 5.4 KCl, 1.4 $MgCl_2$, 2 $CaCl_2$, 10 HEPES, 25 D-Glucose, osmolarity 298 mOsm, pH adjusted to 7.35 with NaOH) and divalent cation free-ECS (DCF-ECS, same recipe as for ECS except Ca^{2+} and Mg^{2+} were replaced with 2 mM EGTA) were added to cells with 0.15 mM propidium iodide (PI, MW 668.4 Da, Invitrogen). Groups of single isolated Cx30- or mutant-expressing cells were analyzed

for their ability to uptake PI under physiological (ECS) and no Ca^{2+} or Mg^{2+} (DCF-ECS) conditions. Images were taken under a 20X lens using the Leica microscope and OpenLab software. Isolated GFP-positive cells were quantified in the assay and approximately 60 cells were recorded for each biological replicate. The number of cells that exhibited dye uptake was recorded as a percentage of the total number of GFP-positive cells examined and a two-way ANOVA was performed on the averages of 4 replicates. For determining cell integrity a dextran-rhodamine-B (DR, 10 kDa, Invitrogen) uptake assay was performed. Cx30-GFP and Briefly, A88V-GFP-expressing cells were incubated in a 0.25% DR-ECS solution, as mentioned above. The number of cells that exhibited dye uptake was recorded as a percentage of the total number of GFP-positive cells and an unpaired Student's *t*-test was performed on the averages of 3 replicates. Values represent the mean percentage of GFP-positive isolated cells that exhibited dye uptake ± s.e.m.

TUNEL Assays

TUNEL assays were performed using an ApopTag® Red *In Situ* Apoptosis Detection Kit (EMD Millipore) as per the manufacturer's instructions with a few modifications. Briefly, control and mutant expressing cells grown in monolayer were fixed in 10% NBF, permeabilized for 10 minutes with 0.5% Triton X-100 in PBS, and subsequently washed with 1X PBS. Following the incubation period with terminal deoxynucleotidyl transferase (TdT) enzyme at 37°C, cells were washed with working strength Stop/Wash buffer twice for 5 minutes each wash. Nuclei were stained with Hoescht 33342 and mounted. Images were obtained using the Leica microscope and OpenLab Software with a 63X oil immersion objective lens. For each biological replicate of transfected cells and controls, 10-15 images were taken of random areas. The percentage of GFP-expressing cells that were positive for ApopTag labelling were calculated per image and a one-way ANOVA was performed on the averages of 3 biological replicates. For untransfected and staurosporin treated controls, the number of ApopTag positive cells was recorded as a percentage of the total cell number. Values represent the mean percentage of apoptotic cells/total number of cells per image ± s.e.m.

XBP-1 reverse-transcriptase (RT)-PCR splicing assay

Processing of X-box binding protein 1 (XBP-1), a marker of ER stress, was detected by PCR and restriction site analysis, as described elsewhere (Williams and Lipkin, 2006). Briefly, REKs were transfected with cDNA encoding Cx30 or mutants 12-24 hrs prior to RNA extraction. As a positive control, untransfected cells were treated with the ER stress-inducing compound tunicamycin (10 µg/ml) for 4-6 hrs prior to RNA extraction. Total RNA was isolated from REKs and RT-PCR performed with RNeasy Mini and OneStep RT-PCR kits (Qiagen, Mississauga, ON), according to the manufacturer's instructions. Briefly, 1 µg of template RNA was reverse transcribed into cDNA in the first step of the RT-PCR cycle (50^{o}C, 30 mins) followed by amplification of the 601 bp XBP-1 product, which encompasses the 26 bp intron sequence containing the *Pst*I restriction site, with the following primers: sense, 5'-AAACAGAGTAGCAGCGCAGACTGC-3'; and antisense, 5'-GGATCTCTAAAACTAGAGGCTTGGTG-3' for 35 cycles at 94^{o}C for 1 min, 60^{o}C for 1 min, and 72^{o}C for 1 min. To confirm GFP-tagged Cx30 or Cx30 mutant expression, separate RT-PCR reactions with the following primers were performed to amplify a 315 bp eGFP product: sense, 5'-TCGTGACCACCCTGACCTAC-3'; and antisense, 5'-AGTTCACCTTGATGCCGTTC-3' for 35 cycles at 94^{o}C for 1 min, 50^{o}C for 1 min, and 72^{o}C for 1 min. Negative controls without RNA template were included in every experiment. To determine whether the XBP-1 products were spliced, half of the cDNA samples were incubated with *Pst*I restriction enzymes at 37^{o}C for 2 hrs. All samples were resolved on 2% agarose gels and densitometry performed on the bands using ImageJ (http://rsb.info.nih.gov/ij/).

Western Blotting

Cell lysates were collected from cultures using a Triton-based extraction buffer [1% Triton X-100 (Sigma Aldrich), 150 mM NaCl, 10 mM Tris, 1 mM EDTA, 1 mM ethylene glycol tetraacetic acid (EGTA), 0.5% nonyl phenoxypolyethoxylethanol (NP-40), 100 mM NaF, 100 mM sodium orthovanadate and proteinase inhibitor mini-EDTA tablet (Roche Applied Science, Laval, QC)] adjusted to pH 7.4 as previously described by Stewart et al (2013). Extractions were repeated 3 times, and protein lysate concentrations were quantified using a bicinchoninic acid (BCA) protein determination kit (Thermo Scientific, Rockford, IL). Total protein lysates of 50 µg were resolved by sodium dodecyl sulfate polyacrylamide gel electrophoresis (SDS-PAGE) on 10% polyacrylamide gels and transferred to nitrocellulose membranes using the iBlot Dry

Blotting System (Invitrogen). Membranes were blocked using 5% Blotto Non-Fat Dry Milk (Santa Cruz Biotechnology) with 0.05% Tween 20 (Sigma Aldrich) in PBS (PBS-T) for 30-60 mins, and subsequently incubated overnight at 4°C with rabbit anti-Cx30 (1:750-1000, Invitrogen), rabbit anti-Cx43 (1:5000, Sigma Aldrich), goat anti-GRP78 (1:500, Santa Cruz Biotechnology), mouse anti-CHOP (3 µg/mL, Abcam, Toronto, ON) and mouse anti-ATF4 (5 µg/mL, Abcam) primary antibodies. Gel loading controls included probing for the levels of β-tubulin using mouse anti-β-tubulin primary antibody (1:10000, Sigma Aldrich). Blots probed for Cx30 were counterstained with mouse anti-GFP antibodies (1:2500, EMD Millipore) to validate that the GFP tag was attached to Cx30 and Cx30 mutants. After several washes with PBS-T, blots were then incubated with secondary anti-rabbit and anti-goat Alexa Fluor 680 (1:5000, Invitrogen) and anti-mouse IRdye 800 (1:5000, LI-COR Biosciences, Lincoln, NE) secondary antibodies for 45-60 minutes. Following more PBS-T washes, blots were scanned and densitometry measurements were quantified using the Odyssey Infrared Imaging System (LI-COR Biosciences). Each signal was normalized to its β-tubulin loading control in the same lane, and the wild type/β-tubulin, GFP/β-tubulin or Cx30/β-tubulin outcome value was set to 1. Unpaired t-tests were performed on the fold change averages of these values from 3 distinct sets of protein lysates. Values represent fold change ± s.e.m.

ACKNOWLEDGEMENTS

We would like to thank Dr. Christian C. Naus for providing us with the pBluescript vector, as well as Dr. Vincent C. Hascall for providing us with the REKs used in this study. We would like to acknowledge Jessica Riley for her contributions to making the Cx30 mutant constructs.

FOOTNOTES

Author contributions

A.C.B., J.J.K., C.S. and D.W.L. designed and interpreted this work. A.C.B. and J.J.K performed the experiments, analyzed the data and wrote the manuscript. J.J.K. and D.W.L. revised the article. P.L. supplied DNA constructs and gave advice and assistance with the UPR experiments.

Funding

This study was supported by a Natural Sciences Engineering Research Council of Canada CGS-M to A.C.B. and by the Canadian Institutes of Health Research to D.W.L.

REFERENCES

Ahmad, S., Chen, S., Sun, J. and Lin, X. (2003). Connexins 26 and 30 are co-assembled to form gap junctions in the cochlea of mice. *Biochem Biophys Res Commun* **307**, 362-8.

Alapure, B. V., Stull, J. K., Firtina, Z. and Duncan, M. K. (2012). The unfolded protein response is activated in connexin 50 mutant mouse lenses. *Exp Eye Res* **102**, 28-37.

Alexander, D. B. and Goldberg, G. S. (2003). Transfer of biologically important molecules between cells through gap junction channels. *Curr Med Chem* **10**, 2045-58.

Anselmi, F., Hernandez, V. H., Crispino, G., Seydel, A., Ortolano, S., Roper, S. D., Kessaris, N., Richardson, W., Rickheit, G., Filippov, M. A. et al. (2008). ATP release through connexin hemichannels and gap junction transfer of second messengers propagate Ca2+ signals across the inner ear. *Proc Natl Acad Sci U S A* **105**, 18770-5.

Bakirtzis, G., Choudhry, R., Aasen, T., Shore, L., Brown, K., Bryson, S., Forrow, S., Tetley, L., Finbow, M., Greenhalgh, D. et al. (2003). Targeted epidermal expression of mutant Connexin 26(D66H) mimics true Vohwinkel syndrome and provides a model for the pathogenesis of dominant connexin disorders. *Hum Mol Genet* **12**, 1737-44.

Baris, H. N., Zlotogorski, A., Peretz-Amit, G., Doviner, V., Shohat, M., Reznik-Wolf, H. and Pras, E. (2008). A novel GJB6 missense mutation in hidrotic ectodermal dysplasia 2 (Clouston syndrome) broadens its genotypic basis. *Br J Dermatol* **159**, 1373-6.

Berridge, M. J. (2002). The endoplasmic reticulum: a multifunctional signaling organelle. *Cell Calcium* **32**, 235-49.

Beyer, E. C., Lin, X. and Veenstra, R. D. (2013). Interfering amino terminal peptides and functional implications for heteromeric gap junction formation. *Front Pharmacol* **4**, 67.

Bitner-Glindzicz, M. (2002). Hereditary deafness and phenotyping in humans. *Br Med Bull* **63**, 73-94.

Boulay, A. C., Del Castillo, F. J., Giraudet, F., Hamard, G., Giaume, C., Petit, C., Avan, P. and Cohen-Salmon, M. (2013). Hearing Is Normal without Connexin30. *J Neurosci* **33**, 430-434.

Burra, S. and Jiang, J. X. (2011). Regulation of cellular function by connexin hemichannels. *Int J Biochem Mol Biol* **2**, 119-128.

Calfon, M., Zeng, H., Urano, F., Till, J. H., Hubbard, S. R., Harding, H. P., Clark, S. G. and Ron, D. (2002). IRE1 couples endoplasmic reticulum load to secretory capacity by processing the XBP-1 mRNA. *Nature* **415**, 92-6.

Chang, Q., Tang, W., Ahmad, S., Stong, B., Leu, G. and Lin, X. (2009). Functional studies reveal new mechanisms for deafness caused by connexin mutations. *Otol Neurotol* **30**, 237-40.

Chang, Q., Tang, W., Ahmad, S., Zhou, B. and Lin, X. (2008). Gap junction mediated intercellular metabolite transfer in the cochlea is compromised in connexin30 null mice. *PLoS One* **3**, e4088.

Chen, N., Xu, C., Han, B., Wang, Z. Y., Song, Y. L., Li, S., Zhang, R. L., Pan, C. M. and Zhang, L. (2010). G11R mutation in GJB6 gene causes hidrotic ectodermal dysplasia involving only hair and nails in a Chinese family. *J Dermatol* **37**, 559-61.

Choudhry, R., Pitts, J. D. and Hodgins, M. B. (1997). Changing patterns of gap junctional intercellular communication and connexin distribution in mouse epidermis and hair follicles during embryonic development. *Dev Dyn* **210**, 417-30.

Christianson, A. L. and Fourie, S. (1996). Family with autosomal dominant hidrotic ectodermal dysplasia: a previously unrecognised syndrome? *Am J Med Genet* **63**, 549-53.

Churko, J. M. and Laird, D. W. (2013). Gap junction remodeling in skin repair following wounding and disease. *Physiology (Bethesda)* **28**, 190-8.

Common, J. E., Becker, D., Di, W. L., Leigh, I. M., O'Toole, E. A. and Kelsell, D. P. (2002). Functional studies of human skin disease- and deafness-associated connexin 30 mutations. *Biochem Biophys Res Commun* **298**, 651-6.

Das Sarma, J., Wang, F. and Koval, M. (2002). Targeted gap junction protein constructs reveal connexin-specific differences in oligomerization. *J Biol Chem* **277**, 20911-8.

de Freitas Junior, J. C., Silva Bdu, R., de Souza, W. F., de Araujo, W. M., Abdelhay, E. S. and Morgado-Diaz, J. A. (2011). Inhibition of N-linked glycosylation by tunicamycin induces E-cadherin-mediated cell-cell adhesion and inhibits cell proliferation in undifferentiated human colon cancer cells. *Cancer Chemother Pharmacol* **68**, 227-38.

De Vuyst, E., Decrock, E., De Bock, M., Yamasaki, H., Naus, C. C., Evans, W. H. and Leybaert, L. (2007). Connexin hemichannels and gap junction channels are differentially influenced by lipopolysaccharide and basic fibroblast growth factor. *Mol Biol Cell* **18**, 34-46.

Decrock, E., De Vuyst, E., Vinken, M., Van Moorhem, M., Vranckx, K., Wang, N., Van Laeken, L., De Bock, M., D'Herde, K., Lai, C. P. et al. (2009). Connexin 43 hemichannels contribute to the propagation of apoptotic cell death in a rat C6 glioma cell model. *Cell Death Differ* **16**, 151-63.

Di, W. L., Monypenny, J., Common, J. E., Kennedy, C. T., Holland, K. A., Leigh, I. M., Rugg, E. L., Zicha, D. and Kelsell, D. P. (2002). Defective trafficking and cell death is characteristic of skin disease-associated connexin 31 mutations. *Hum Mol Genet* **11**, 2005-14.

Di, W. L., Rugg, E. L., Leigh, I. M. and Kelsell, D. P. (2001). Multiple epidermal connexins are expressed in different keratinocyte subpopulations including connexin 31. *J Invest Dermatol* **117**, 958-64.

Essenfelder, G. M., Bruzzone, R., Lamartine, J., Charollais, A., Blanchet-Bardon, C., Barbe, M. T., Meda, P. and Waksman, G. (2004). Connexin30 mutations responsible for hidrotic ectodermal dysplasia cause abnormal hemichannel activity. *Hum Mol Genet* **13**, 1703-14.

Evans, W. H., Ahmad, S., Diez, J., George, C. H., Kendall, J. M. and Martin, P. E. (1999). Trafficking pathways leading to the formation of gap junctions. *Novartis Found Symp* **219**, 44-54; discussion 54-9.

Forge, A., Marziano, N. K., Casalotti, S. O., Becker, D. L. and Jagger, D. (2003). The inner ear contains heteromeric channels composed of cx26 and cx30 and deafness-related mutations in cx26 have a dominant negative effect on cx30. *Cell Commun Adhes* **10**, 341-6.

Fraser, F. C. and Der Kaloustian, V. M. (2001). A man, a syndrome, a gene: Clouston's hidrotic ectodermal dysplasia (HED). *Am J Med Genet* **100**, 164-8.

Galehdar, Z., Swan, P., Fuerth, B., Callaghan, S. M., Park, D. S. and Cregan, S. P. (2010). Neuronal apoptosis induced by endoplasmic reticulum stress is regulated by ATF4-

CHOP-mediated induction of the Bcl-2 homology 3-only member PUMA. *J Neurosci* **30**, 16938-48.

Gerido, D. A., DeRosa, A. M., Richard, G. and White, T. W. (2007). Aberrant hemichannel properties of Cx26 mutations causing skin disease and deafness. *Am J Physiol Cell Physiol* **293**, C337-45.

Gong, X. Q., Shao, Q., Langlois, S., Bai, D. and Laird, D. W. (2007). Differential potency of dominant negative connexin43 mutants in oculodentodigital dysplasia. *J Biol Chem* **282**, 19190-202.

Gossman, D. G. and Zhao, H. B. (2008). Hemichannel-mediated inositol 1,4,5-trisphosphate (IP3) release in the cochlea: a novel mechanism of IP3 intercellular signaling. *Cell Commun Adhes* **15**, 305-15.

Grifa, A., Wagner, C. A., D'Ambrosio, L., Melchionda, S., Bernardi, F., Lopez-Bigas, N., Rabionet, R., Arbones, M., Monica, M. D., Estivill, X. et al. (1999). Mutations in GJB6 cause nonsyndromic autosomal dominant deafness at DFNA3 locus. *Nat Genet* **23**, 16-8.

Groenendyk, J. and Michalak, M. (2005). Endoplasmic reticulum quality control and apoptosis. *Acta Biochim Pol* **52**, 381-95.

Harris, A. L. (2007). Connexin channel permeability to cytoplasmic molecules. *Prog Biophys Mol Biol* **94**, 120-43.

He, L. Q., Liu, Y., Cai, F., Tan, Z. P., Pan, Q., Liang, D. S., Long, Z. G., Wu, L. Q., Huang, L. Q., Dai, H. P. et al. (2005). Intracellular distribution, assembly and effect of disease-associated connexin 31 mutants in HeLa cells. *Acta Biochim Biophys Sin (Shanghai)* **37**, 547-54.

Hidvegi, T., Schmidt, B. Z., Hale, P. and Perlmutter, D. H. (2005). Accumulation of mutant alpha1-antitrypsin Z in the endoplasmic reticulum activates caspases-4 and -12, NFkappaB, and BAP31 but not the unfolded protein response. *J Biol Chem* **280**, 39002-15.

Hoang Dinh, E., Ahmad, S., Chang, Q., Tang, W., Stong, B. and Lin, X. (2009). Diverse deafness mechanisms of connexin mutations revealed by studies using in vitro approaches and mouse models. *Brain Res* **1277**, 52-69.

Huang, T., Shao, Q., MacDonald, A., Xin, L., Lorentz, R., Bai, D. and Laird, D. W. (2013). Autosomal recessive GJA1 (Cx43) gene mutations cause oculodentodigital dysplasia by distinct mechanisms. *J Cell Sci* **126**, 2857-66.

Jan, A. Y., Amin, S., Ratajczak, P., Richard, G. and Sybert, V. P. (2004). Genetic heterogeneity of KID syndrome: identification of a Cx30 gene (GJB6) mutation in a patient with KID syndrome and congenital atrichia. *J Invest Dermatol* **122**, 1108-13.

Jara, O., Acuna, R., Garcia, I. E., Maripillan, J., Figueroa, V., Saez, J. C., Araya-Secchi, R., Lagos, C. F., Perez-Acle, T., Berthoud, V. M. et al. (2012). Critical role of the first transmembrane domain of Cx26 in regulating oligomerization and function. *Mol Biol Cell* **23**, 3299-311.

Jordan, K., Solan, J. L., Dominguez, M., Sia, M., Hand, A., Lampe, P. D. and Laird, D. W. (1999). Trafficking, assembly, and function of a connexin43-green fluorescent protein chimera in live mammalian cells. *Mol Biol Cell* **10**, 2033-50.

Kalvelyte, A., Imbrasaite, A., Bukauskiene, A., Verselis, V. K. and Bukauskas, F. F. (2003). Connexins and apoptotic transformation. *Biochem Pharmacol* **66**, 1661-72.

Kibar, Z., Dube, M. P., Powell, J., McCuaig, C., Hayflick, S. J., Zonana, J., Hovnanian, A., Radhakrishna, U., Antonarakis, S. E., Benohanian, A. et al. (2000). Clouston hidrotic ectodermal dysplasia (HED): genetic homogeneity, presence of a founder effect in the French Canadian population and fine genetic mapping. *Eur J Hum Genet* **8**, 372-80.

Kikuchi, T., Adams, J. C., Miyabe, Y., So, E. and Kobayashi, T. (2000). Potassium ion recycling pathway via gap junction systems in the mammalian cochlea and its interruption in hereditary nonsyndromic deafness. *Med Electron Microsc* **33**, 51-6.

Kleizen, B. and Braakman, I. (2004). Protein folding and quality control in the endoplasmic reticulum. *Curr Opin Cell Biol* **16**, 343-9.

Koval, M. (2006). Pathways and control of connexin oligomerization. *Trends Cell Biol* **16**, 159-66.

Koval, M., Harley, J. E., Hick, E. and Steinberg, T. H. (1997). Connexin46 is retained as monomers in a trans-Golgi compartment of osteoblastic cells. *J Cell Biol* **137**, 847-57.

Kretz, M., Maass, K. and Willecke, K. (2004). Expression and function of connexins in the epidermis, analyzed with transgenic mouse mutants. *Eur J Cell Biol* **83**, 647-54.

Kumar, N. M. and Gilula, N. B. (1996). The gap junction communication channel. *Cell* **84**, 381-8.

Kwon, T., Harris, A. L., Rossi, A. and Bargiello, T. A. (2011). Molecular dynamics simulations of the Cx26 hemichannel: evaluation of structural models with Brownian dynamics. *J Gen Physiol* **138**, 475-93.

Lai, A., Le, D. N., Paznekas, W. A., Gifford, W. D., Jabs, E. W. and Charles, A. C. (2006). Oculodentodigital dysplasia connexin43 mutations result in non-functional connexin hemichannels and gap junctions in C6 glioma cells. *J Cell Sci* **119**, 532-41.

Laird, D. W. (2006). Life cycle of connexins in health and disease. *Biochem J* **394**, 527-43.

Laird, D. W., Jordan, K. and Shao, Q. (2001). Expression and imaging of connexin-GFP chimeras in live mammalian cells. *Methods Mol Biol* **154**, 135-42.

Lamartine, J., Munhoz Essenfelder, G., Kibar, Z., Lanneluc, I., Callouet, E., Laoudj, D., Lemaitre, G., Hand, C., Hayflick, S. J., Zonana, J. et al. (2000). Mutations in GJB6 cause hidrotic ectodermal dysplasia. *Nat Genet* **26**, 142-4.

Langlois, S., Maher, A. C., Manias, J. L., Shao, Q., Kidder, G. M. and Laird, D. W. (2007). Connexin levels regulate keratinocyte differentiation in the epidermis. *J Biol Chem* **282**, 30171-80.

Lee, J. R., Derosa, A. M. and White, T. W. (2009). Connexin mutations causing skin disease and deafness increase hemichannel activity and cell death when expressed in Xenopus oocytes. *J Invest Dermatol* **129**, 870-8.

Maeda, S., Nakagawa, S., Suga, M., Yamashita, E., Oshima, A., Fujiyoshi, Y. and Tsukihara, T. (2009). Structure of the connexin 26 gap junction channel at 3.5 A resolution. *Nature* **458**, 597-602.

Maher, A. C., Thomas, T., Riley, J. L., Veitch, G., Shao, Q. and Laird, D. W. (2005). Rat epidermal keratinocytes as an organotypic model for examining the role of Cx43 and Cx26 in skin differentiation. *Cell Commun Adhes* **12**, 219-30.

Malhotra, J. D. and Kaufman, R. J. (2007). The endoplasmic reticulum and the unfolded protein response. *Semin Cell Dev Biol* **18**, 716-31.

Marziano, N. K., Casalotti, S. O., Portelli, A. E., Becker, D. L. and Forge, A. (2003). Mutations in the gene for connexin 26 (GJB2) that cause hearing loss have a dominant negative effect on connexin 30. *Hum Mol Genet* **12**, 805-12.

McLachlan, E., Shao, Q. and Laird, D. W. (2007). Connexins and gap junctions in mammary gland development and breast cancer progression. *J Membr Biol* **218**, 107-21.

Mese, G., Sellitto, C., Li, L., Wang, H. Z., Valiunas, V., Richard, G., Brink, P. R. and White, T. W. (2011). The Cx26-G45E mutation displays increased hemichannel activity in a mouse model of the lethal form of keratitis-ichthyosis-deafness syndrome. *Mol Biol Cell* **22**, 4776-86.

Mhaske, P. V., Levit, N. A., Li, L., Wang, H. Z., Lee, J. R., Shuja, Z., Brink, P. R. and White, T. W. (2013). The human Cx26-D50A and Cx26-A88V mutations causing keratitis-ichthyosis-deafness syndrome display increased hemichannel activity. *Am J Physiol Cell Physiol* **304**, C1150-8.

Miwa, T., Minoda, R., Ise, M., Yamada, T. and Yumoto, E. (2013). Mouse Otocyst Transuterine Gene Transfer Restores Hearing in Mice With Connexin 30 Deletion-associated Hearing Loss. *Mol Ther* **21**, 1142-50.

Musil, L. S. and Goodenough, D. A. (1993). Multisubunit assembly of an integral plasma membrane channel protein, gap junction connexin43, occurs after exit from the ER. *Cell* **74**, 1065-77.

Nemoto-Hasebe, I., Akiyama, M., Kudo, S., Ishiko, A., Tanaka, A., Arita, K. and Shimizu, H. (2009). Novel mutation p.Gly59Arg in GJB6 encoding connexin 30 underlies palmoplantar keratoderma with pseudoainhum, knuckle pads and hearing loss. *Br J Dermatol* **161**, 452-5.

Nickel, R. and Forge, A. (2008). Gap junctions and connexins in the inner ear: their roles in homeostasis and deafness. *Curr Opin Otolaryngol Head Neck Surg* **16**, 452-7.

Pahl, H. L., Sester, M., Burgert, H. G. and Baeuerle, P. A. (1996). Activation of transcription factor NF-kappaB by the adenovirus E3/19K protein requires its ER retention. *J Cell Biol* **132**, 511-22.

Penuela, S., Bhalla, R., Gong, X. Q., Cowan, K. N., Celetti, S. J., Cowan, B. J., Bai, D., Shao, Q. and Laird, D. W. (2007). Pannexin 1 and pannexin 3 are glycoproteins that exhibit many distinct characteristics from the connexin family of gap junction proteins. *J Cell Sci* **120**, 3772-83.

Rasheva, V. I. and Domingos, P. M. (2009). Cellular responses to endoplasmic reticulum stress and apoptosis. *Apoptosis* **14**, 996-1007.

Richard, G., Brown, N., Ishida-Yamamoto, A. and Krol, A. (2004). Expanding the phenotypic spectrum of Cx26 disorders: Bart-Pumphrey syndrome is caused by a novel missense mutation in GJB2. *J Invest Dermatol* **123**, 856-63.

Ron, D. and Walter, P. (2007). Signal integration in the endoplasmic reticulum unfolded protein response. *Nat Rev Mol Cell Biol* **8**, 519-29.

Rouan, F., White, T. W., Brown, N., Taylor, A. M., Lucke, T. W., Paul, D. L., Munro, C. S., Uitto, J., Hodgins, M. B. and Richard, G. (2001). Trans-dominant inhibition of connexin-43 by mutant connexin-26: implications for dominant connexin disorders affecting epidermal differentiation. *J Cell Sci* **114**, 2105-13.

Saraste, A. and Pulkki, K. (2000). Morphologic and biochemical hallmarks of apoptosis. *Cardiovasc Res* **45**, 528-37.

Schutz, M., Scimemi, P., Majumder, P., De Siati, R. D., Crispino, G., Rodriguez, L., Bortolozzi, M., Santarelli, R., Seydel, A., Sonntag, S. et al. (2010). The human deafness-associated connexin 30 T5M mutation causes mild hearing loss and reduces biochemical coupling among cochlear non-sensory cells in knock-in mice. *Hum Mol Genet* **19**, 4759-73.

Smith, F. J., Morley, S. M. and McLean, W. H. (2002). A novel connexin 30 mutation in Clouston syndrome. *J Invest Dermatol* **118**, 530-2.

Sohl, G. and Willecke, K. (2003). An update on connexin genes and their nomenclature in mouse and man. *Cell Commun Adhes* **10**, 173-80.

Sohl, G. and Willecke, K. (2004). Gap junctions and the connexin protein family. *Cardiovasc Res* **62**, 228-32.

Stewart, M. K., Gong, X. Q., Barr, K. J., Bai, D., Fishman, G. I. and Laird, D. W. (2013). The severity of mammary gland developmental defects is linked to the overall functional status of Cx43 as revealed by genetically modified mice. *Biochem J* **449**, 401-13.

Stong, B. C., Chang, Q., Ahmad, S. and Lin, X. (2006). A novel mechanism for connexin 26 mutation linked deafness: cell death caused by leaky gap junction hemichannels. *Laryngoscope* **116**, 2205-10.

Stout, C. E., Costantin, J. L., Naus, C. C. and Charles, A. C. (2002). Intercellular calcium signaling in astrocytes via ATP release through connexin hemichannels. *J Biol Chem* **277**, 10482-8.

Subramanian, K. and Meyer, T. (1997). Calcium-induced restructuring of nuclear envelope and endoplasmic reticulum calcium stores. *Cell* **89**, 963-71.

Sugiura, K., Muro, Y., Futamura, K., Matsumoto, K., Hashimoto, N., Nishizawa, Y., Nagasaka, T., Saito, H., Tomita, Y. and Usukura, J. (2009). The unfolded protein response is activated in differentiating epidermal keratinocytes. *J Invest Dermatol* **129**, 2126-35.

Tang, Q., Dowd, T. L., Verselis, V. K. and Bargiello, T. A. (2009). Conformational changes in a pore-forming region underlie voltage-dependent "loop gating" of an unapposed connexin hemichannel. *J Gen Physiol* **133**, 555-70.

Tattersall, D., Scott, C. A., Gray, C., Zicha, D. and Kelsell, D. P. (2009). EKV mutant connexin 31 associated cell death is mediated by ER stress. *Hum Mol Genet* **18**, 4734-45.

Teubner, B., Michel, V., Pesch, J., Lautermann, J., Cohen-Salmon, M., Sohl, G., Jahnke, K., Winterhager, E., Herberhold, C., Hardelin, J. P. et al. (2003). Connexin30 (Gjb6)-deficiency causes severe hearing impairment and lack of endocochlear potential. *Hum Mol Genet* **12**, 13-21.

Thomas, T., Shao, Q. and Laird, D. W. (2007). Differentiation of organotypic epidermis in the presence of skin disease-linked dominant-negative Cx26 mutants and knockdown Cx26. *J Membr Biol* **217**, 93-104.

Thomas, T., Telford, D. and Laird, D. W. (2004). Functional domain mapping and selective trans-dominant effects exhibited by Cx26 disease-causing mutations. *J Biol Chem* **279**, 19157-68.

Tong, D., Li, T. Y., Naus, K. E., Bai, D. and Kidder, G. M. (2007). In vivo analysis of undocked connexin43 gap junction hemichannels in ovarian granulosa cells. *J Cell Sci* **120**, 4016-24.

Valiunas, V. and Weingart, R. (2000). Electrical properties of gap junction hemichannels identified in transfected HeLa cells. *Pflugers Arch* **440**, 366-79.

Verselis, V. K. and Srinivas, M. (2008). Divalent cations regulate connexin hemichannels by modulating intrinsic voltage-dependent gating. *J Gen Physiol* **132**, 315-27.

Verselis, V. K., Trelles, M. P., Rubinos, C., Bargiello, T. A. and Srinivas, M. (2009). Loop gating of connexin hemichannels involves movement of pore-lining residues in the first extracellular loop domain. *J Biol Chem* **284**, 4484-93.

Wang, W. H., Liu, Y. F., Su, C. C., Su, M. C., Li, S. Y. and Yang, J. J. (2011). A novel missense mutation in the connexin30 causes nonsyndromic hearing loss. *PLoS One* **6**, e21473.

Wangemann, P. (2006). Supporting sensory transduction: cochlear fluid homeostasis and the endocochlear potential. *J Physiol* **576**, 11-21.

Williams, B. L. and Lipkin, W. I. (2006). Endoplasmic reticulum stress and neurodegeneration in rats neonatally infected with borna disease virus. *J Virol* **80**, 8613-26.

Yum, S. W., Zhang, J., Valiunas, V., Kanaporis, G., Brink, P. R., White, T. W. and Scherer, S. S. (2007). Human connexin26 and connexin30 form functional heteromeric and heterotypic channels. *Am J Physiol Cell Physiol* **293**, C1032-48.

Zhang, X. J., Chen, J. J., Yang, S., Cui, Y., Xiong, X. Y., He, P. P., Dong, P. L., Xu, S. J., Li, Y. B., Zhou, Q. et al. (2003). A mutation in the connexin 30 gene in Chinese Han patients with hidrotic ectodermal dysplasia. *J Dermatol Sci* **32**, 11-7.

Zhang, Y., Tang, W., Ahmad, S., Sipp, J. A., Chen, P. and Lin, X. (2005). Gap junction-mediated intercellular biochemical coupling in cochlear supporting cells is required for normal cochlear functions. *Proc Natl Acad Sci U S A* **102**, 15201-6.

Zhao, H. B., Kikuchi, T., Ngezahayo, A. and White, T. W. (2006). Gap junctions and cochlear homeostasis. *J Membr Biol* **209**, 177-86.

Zhao, H. B., Yu, N. and Fleming, C. R. (2005). Gap junctional hemichannel-mediated ATP release and hearing controls in the inner ear. *Proc Natl Acad Sci U S A* **102**, 18724-9.

FIGURE LEGENDS

Figure 1. Cx30 mutations linked to hearing loss and skin diseases, and their differential ectopic expression in REKs. **(A)** Schematic diagram of Cx30 depicting four mutations associated with hearing loss (yellow), hearing loss plus skin disease (orange) and skin disease (green). **(B)** Western blot analysis was used to detect the levels of GFP-tagged Cx30 and Cx30 mutants when ectopically expressed in REKs. Blots were probed with anti-Cx30, anti-GFP or anti-β-tubulin antibodies. **(C)** Anti-GFP labeling revealed significantly lower levels of GFP-tagged V37E and A88V mutants compared to the levels of wild-type Cx30. Values represent fold change ± s.e.m. (unpaired t-test, $^{**}P<0.01$, N=3).

Figure 2. Skin disease-linked Cx30 mutants have impaired abilities to form gap junction plaques. **(A)** Untransfected REKs and REKs ectopically expressing GFP-tagged Cx30 or Cx30 mutants (green) were immunolabeled for protein disulfide isomerase (PDI) (red) to denote the ER. Nuclei were stained with Hoescht 33342 (blue). Cx30 and the T5M mutant formed punctate gap junction-like structures at the cell-to-cell interface, while V37E co-localized with PDI. The G59R and A88V mutants were primarily localized in intracellular compartments, however a population of the mutants did reside at the cell surface (white arrows). PDI staining

was absent in A88V mutant-expressing cells, and GFP-positive cells without nuclei were dead "ghost" cells. Scale bar = 20 μm. **(B)** Immunolabeling REKs for Cx30 (green) revealed that untagged mutant expressing cells exhibited similar localization profiles as GFP-tagged mutants. Similarly, populations of the G59R and A88V mutants localized to the cell surface (arrows). Scale bar = 20 μm. **(C)** REKs ectopically expressing the G59R mutant were double-labeled for Cx30 (green) and Golgi matrix protein 130 (GM130) (red), which revealed that the G59R mutant co-localized with the Golgi apparatus. Scale bar = 20 μm.

Figure 3. Effect of Cx30 mutants on endogenous Cx43 in REKs (A) Cx30- and Cx30 mutant-expressing REKs (green) were immunolabeled for Cx43 (red) and stained with Hoescht 33342 (blue) to denote cell nuclei. Cx43 plaques were localized at the cell surface between REKs expressing Cx30 or the T5M and G59R mutants. V37E- and A88V-expressing REKs did not exhibit Cx43 plaque formation between apposing cells. Scale bar = 20 μm. **(B)** Western blot analysis was used to detect total levels of Cx43 in Cx30- and mutant-expressing cells when normalized to β-tubulin. **(C)** Total levels of Cx43 were slightly lower in REKs expressing only the T5M hearing loss mutant and remained unchanged in V37E, G59R and A88V mutant-expressing cells. Values represent fold change ± s.e.m. (unpaired Student's *t*-test, $*P<0.05$, N=3).

Figure 4. Skin disease-linked V37E, G59R and A88V mutants differentially affect GJIC when expressed in HeLa cells and REKs. (A) GFP-, Cx30- and mutant-expressing HeLa cells (denoted in phase-contrast images) were imaged for the presence of GFP and microinjected with Alexa 350 dye (red asterisks). Scale bar = 20 μm. **(B)** Relative to Untr control cells, cells expressing Cx30 or the T5M mutant exhibited significantly greater incidence of dye transfer than those expressing the V37E or G59R mutants. **(C)** Untr and GFP-, Cx30- and mutant-expressing REKs (denoted by phase-contrast images) were imaged for the presence of GFP and microinjected with Alexa 350 dye (red asterisks). Scale bar = 20 μm. **(D)** Relative to Untr controls, cells expressing the V37E and A88V mutants exhibited significantly lower incidences of Cx43-mediated dye transfer. Numbers of injected cells are presented along the bottom of the panels (B, D). Values represent the mean percent incidence of dye transfer ± s.e.m. (one-way

ANOVA, $^{**}P<0.01$, $^{***}P<0.001$, N=3). Numbers of injected cells are presented along the bottom of the figure.

Figure 5. The hearing loss-linked T5M mutant exhibits hemichannel activity in HeLa cells that mimics Cx30. (A) Single isolated Cx30- or mutant-expressing HeLa cells (denoted in phase-contrast images) were incubated with propidium iodide (PI) in normal extracellular solution (ECS) or divalent cation free-ECS (DCF-ECS). Cells were imaged for the presence of GFP (green) and PI uptake (red). Scale bar = 20 µm. **(B)** Cells expressing the V37E and G59R mutants did not uptake PI under DCF-ECS conditions, while those expressing Cx30 or the T5M mutant exhibited significant hemichannel activity. (C) The majority of single cells expressing the A88V mutant were permeable to dextran-rhodamine (DR) under ECS conditions, indicating disruption of the cell membrane. Thus, the A88V mutant could not be used in the PI uptake assay. Values represent the mean percentage of GFP-positive isolated cells that exhibited PI or DR uptake ± s.e.m. (B, two-way ANOVA, $^{***}P<0.001$, N=4; C, Student's *t*-test, $^{***}P<0.001$, N=3).

Figure 6. Ectopic expression of Clouston syndrome-linked V37E and A88V mutants induces apoptosis in REKs. (A) TUNEL assays were performed on untransfected (Untr), GFP-, Cx30- and mutant-expressing REKs (green). Nuclei were stained with Hoescht 33342 (blue) and apoptotic cells are indicated by ApopTag staining (red). Staurosporine (Stauro)-treated cells served as an inducer of apoptosis. Scale bar = 20 µm. **(B)** The expression of V37E and A88V mutants significantly induced apoptosis in REKs. (**C**) Treatment with staurosporine significantly induced apoptosis compared to untransfected controls. Values represent the mean percentage of apoptotic cells/total number of cells per image ± s.e.m. (one way ANOVA, $^{***}P<0.001$, N=3).

Figure 7. Cx30 has minimal ability to rescue the trafficking of skin disease-linked mutants to the cell surface in REKs. REKs co-expressing Cx30-RFP (red) together with GFP-tagged Cx30, T5M, V37E, G59R or A88V mutants (green) were stained with Hoescht 33342 (blue) to denote the cell nuclei. Cx30, the T5M mutant and populations of the G59R and A88V mutants distinctly co-localized with Cx30-RFP at the cell surface. Wild-type Cx30 minimally rescued

the trafficking of V37E, G59R and A88V mutants since the majority of the protein was localized to intracellular compartments. Scale bar = 20 μm.

Figure 8. Clouston syndrome-linked Cx30 mutants exhibit a dominant-negative effect on ectopically-expressed Cx26 in REKs. REKs co-expressing Cx26-RFP (red) together with GFP-tagged Cx30, T5M, V37E, G59R or A88V mutants (green) were stained with Hoescht 33342 (blue) to denote the cell nuclei. Cx30, the T5M mutant and a population of the G59R mutant distinctly co-localized with Cx26-RFP at the cell surface. Wild-type Cx26 failed to rescue trafficking of V37E and A88V mutants whereas the majority of the G59R mutant accumulated within intracellular compartments. V37E and A88V Cx30 mutants exhibited a dominant-negative effect on wild-type Cx26, as Cx26-RFP was retained inside the cell and particularly co-localized with the A88V mutant. Scale bar = 20 μm.

Figure S1. Expression of the V37E and A88V mutants reduced the incidents of co-expressed Cx43 being found in gap junctions. HeLa cells were engineered to co-express GFP-tagged Cx30 and T5M, V37E, G59R and A88V mutants (green) with Cx43-RFP (red). Cx30 and T5M showed co-localization in gap junction-like plaques with Cx43. The V37E and A88V mutants showed intracellular accumulations that co-localized with Cx43 and reduced Cx43 plaques were evident. The G59R mutant localized intracellularly, but it did not appear to affect the ability of Cx43 to reach the cell surface. Scale bar = 20 μm.

Figure S2. REKs expressing V37E and A88V mutants express cleaved caspase-3. Untransfected (Untr) cells or GFP-, Cx30- and mutant-expressing REKs (green) were immunolabeled for cleaved caspase-3 (red) and nuclei were stained with Hoescht 33342 (blue). Cells expressing the V37E and A88V mutants also expressed the apoptotic marker cleaved caspase-3. Scale bar = 20 μm.

Figure S3. Western blot analysis of the unfolded protein response in mutant-expressing REKs. The levels of unfolded protein response (UPR) markers glucose regulated protein 78 (GRP78) (A), activating transcription factor 4 (ATF4) (B) and C/EBP homologous protein (CHOP) (C) in untransfected (Untr) and GFP-, Cx30- and mutant-expressing REKs were

analyzed and normalized to β-tubulin. Protein lysates from tunicamycin (Tm)-treated cells served as an inducer of the UPR. Blots were also probed with anti-β-tubulin antibody. Normalized values for Untr cells were set to 1. **(A)** In comparison to GFP-expressing cells, GRP78 expression was significantly higher in Tm-treated controls (***P<0.001) and not in cells expressing the mutants. **(B)** In comparison to GFP-expressing cells, ATF4 expression was higher in V37E-expressing cells (*P<0.05) and Tm-treated controls only (**P<0.01). **(C)** CHOP was also only up-regulated in Tm-treated cells only (*P<0.05 and **P<0.01). Values represent fold change ± s.e.m. (unpaired Student's *t*-test, N=3). **(D, E)** Upon activation, IRE1 cleaves an intron (black box) from XBP1 mRNA to yield a spliced variant without a *Pst*I site. The possible band sizes produced by splicing and *Pst*I digestion are shown in the table. **(F)** RNA from untransfected REKs (Untr), REKs treated with tunicamycin (Tm) and REKs expressing Cx30 or Cx30 mutants was analyzed by RT-PCR using primers that amplified both the spliced (XBP1s) and unspliced (XBP1u) variants. Upper panel shows a representative gel separation of undigested and *Pst*1 digested bands. Note the loss of XBP1u bands (289 bp and 312 bp) and increased intensity of the XBP1s band (575 bp) for the Tm control. All other band intensities were similar between Untr and Cx30 mutants. The lower panel represents a higher resolution image of the *Pst*I undigested bands showing the separation of XBP1u and XBP1s. **(G)** Densitometry quantification and ratio of upper (575-601 bp) to lower (289-312 bp) bands showed no significant increase in XBP1 splicing for any of the mutants, whereas the Tm control significantly induced a ~3.5 fold increase in XBP1s. Values represent fold change ± s.e.m. (one way ANOVA, ***P<0.001, N=6).

Figure S4. Cx30 and Cx26 may partially rescue the trafficking of V37E and A88V mutants in HeLa cells. HeLa cells co-expressing Cx30-RFP (red) together with GFP-tagged Cx30, T5M, V37E, G59R or A88V mutants (green) were stained with Hoescht 33342 (blue) to denote the cell nuclei. Cx30, T5M and populations of the V37E, G59R and A88V mutants distinctly co-localized with Cx30-RFP at the cell surface, however all skin disease-linked mutants were primarily intracellularly localized. HeLa cells co-expressing Cx26-RFP (red) and GFP-tagged Cx30, T5M, V37E, G59R or A88V mutants (green) were stained with Hoescht 33342 (blue) to denote the nuclei. Cx30 and T5M co-localized strongly with Cx26-RFP at the cell surface, as did the G59R mutant. There were marked reductions in Cx26-RFP gap junction plaques in both

V37E and A88V expressing cells and an increase in intracellular Cx26-RFP co-localization. Scale Bars = 20 μm.

A

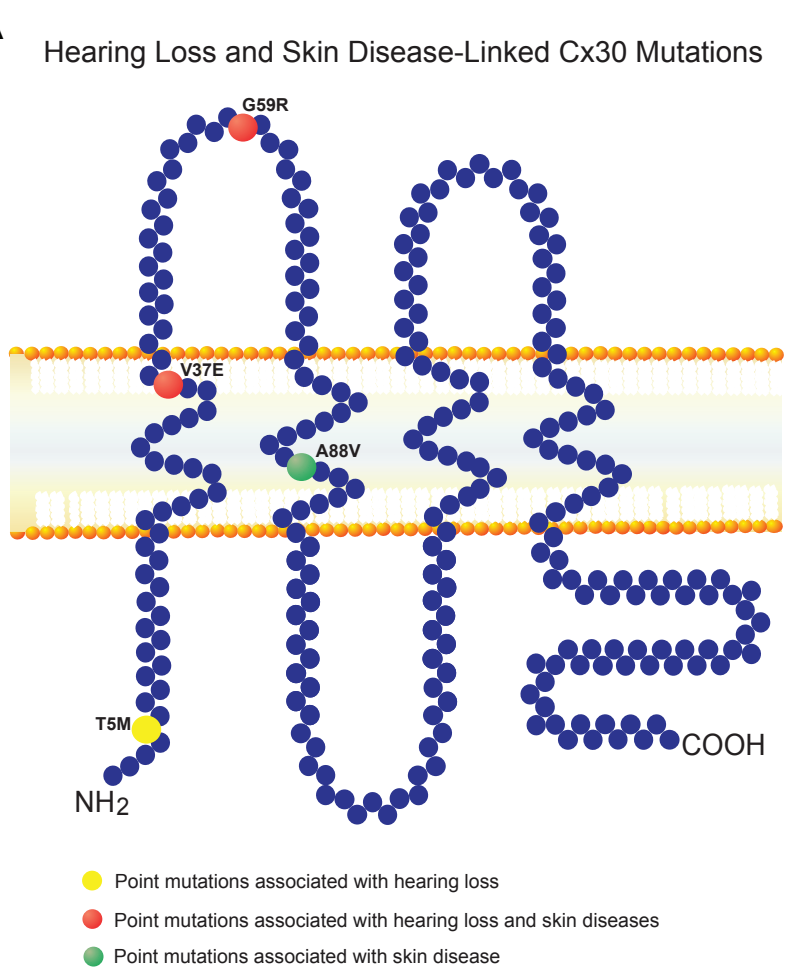
Hearing Loss and Skin Disease-Linked Cx30 Mutations
G59R
V37E
A88V
T5M
COOH
NH2
Point mutations associated with hearing loss
Point mutations associated with hearing loss and skin diseases
Point mutations associated with skin disease

B

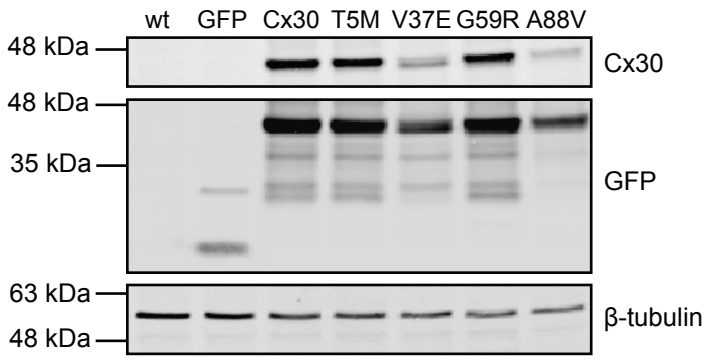
wt
GFP
Cx30
T5M
V37E
G59R
A88V
48 kDa
48 kDa
35 kDa
63 kDa
48 kDa
Cx30
GFP
β-tubulin

C

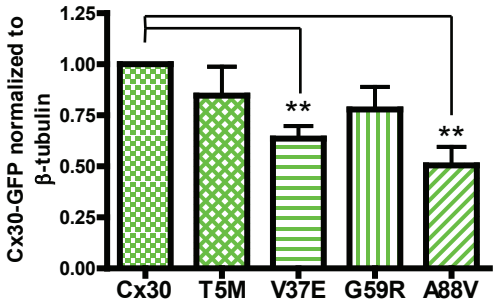
Cx30-GFP normalized to β-tubulin
1.25
1.00
0.75
0.50
0.25
0.00
**
**
Cx30
T5M
V37E
G59R
A88V

FIGURE 1

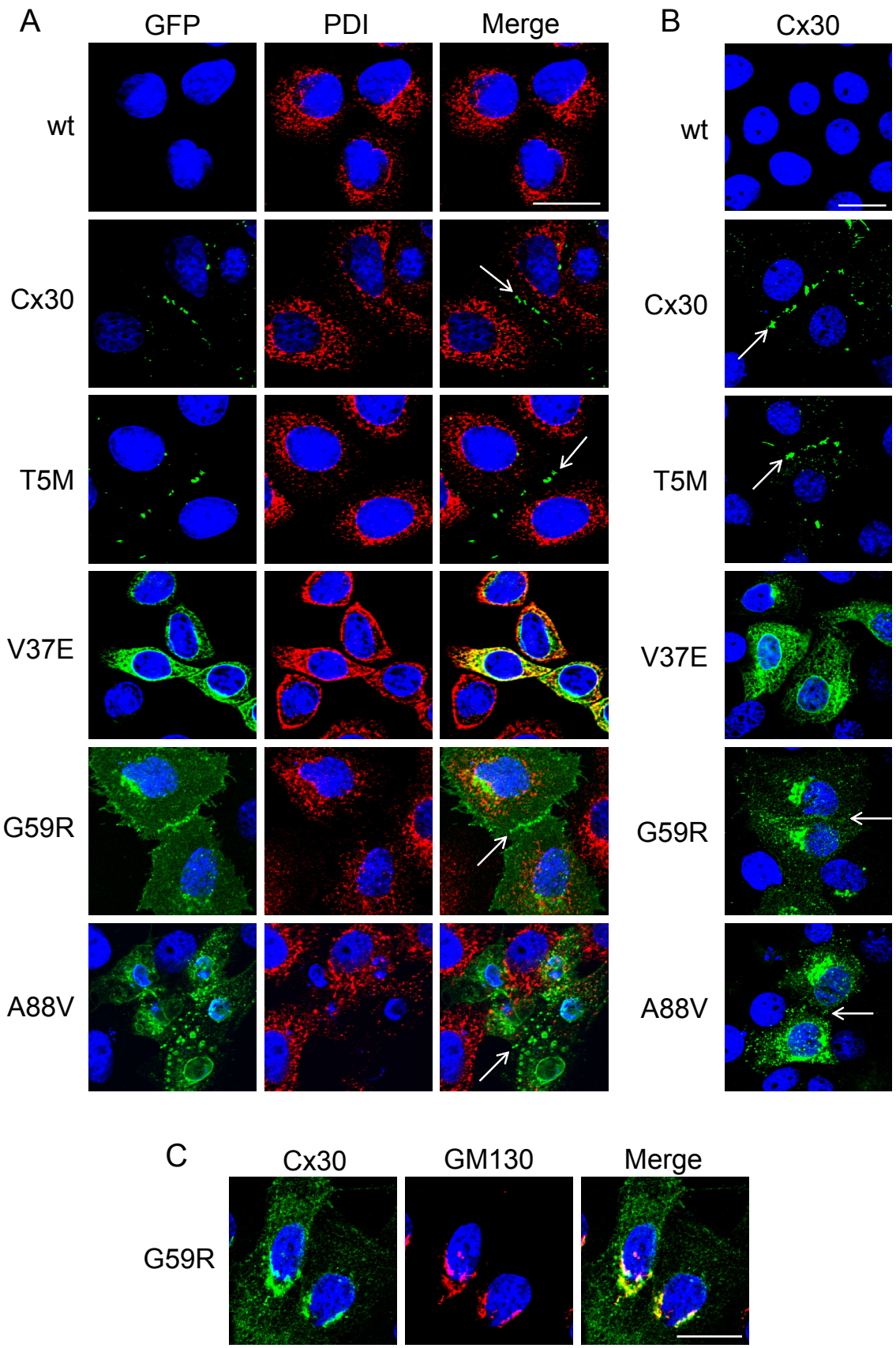
A
GFP
PDI
Merge
B
Cx30
wt
Cx30
T5M
V37E
G59R
A88V
wt
Cx30
T5M
V37E
G59R
A88V
C
Cx30
GM130
Merge
G59R

FIGURE 2

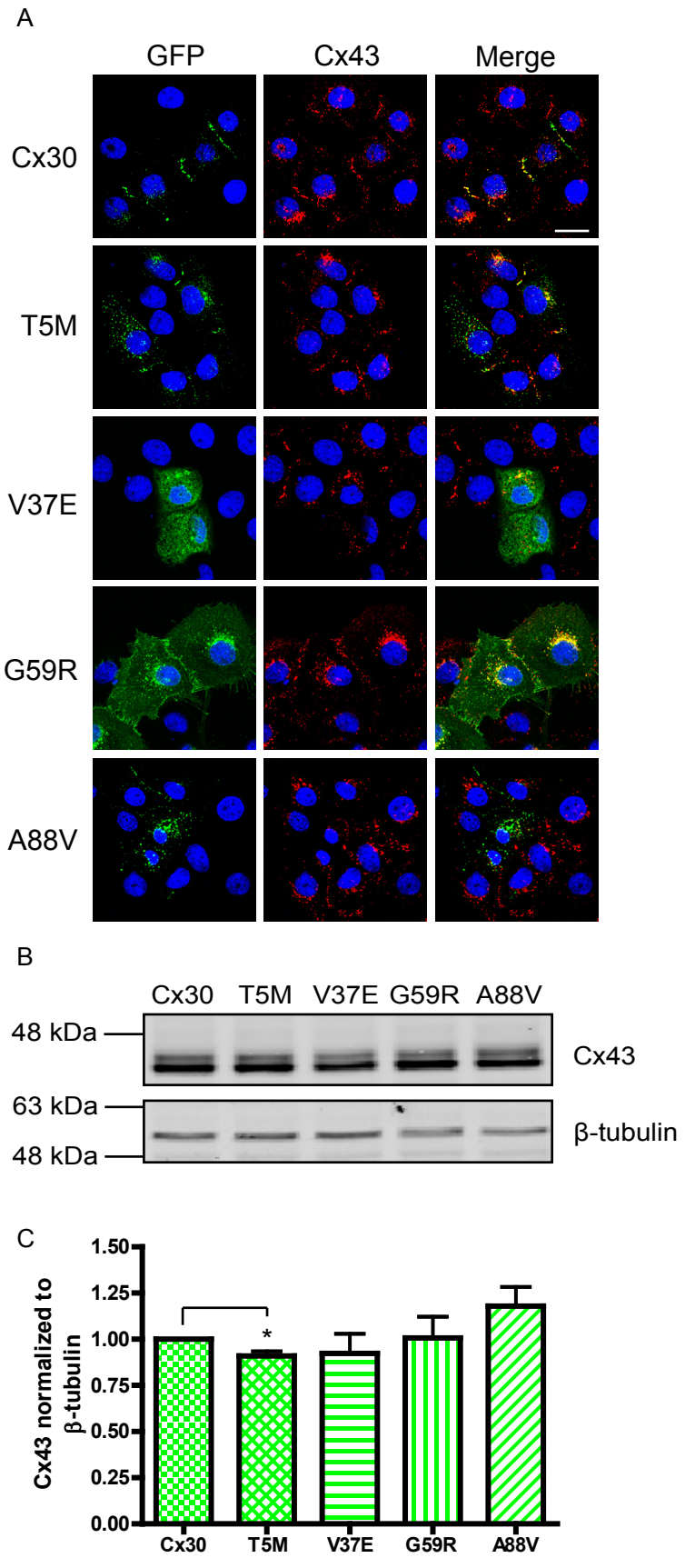
A
GFP
Cx43
Merge
Cx30
T5M
V37E
G59R
A88V
B
Cx30
T5M
V37E
G59R
A88V
48 kDa
Cx43
63 kDa
48 kDa
β-tubulin
C
Cx43 normalized to β-tubulin
1.50
1.25
1.00
0.75
0.50
0.25
0.00
*
Cx30
T5M
V37E
G59R
A88V

FIGURE 3

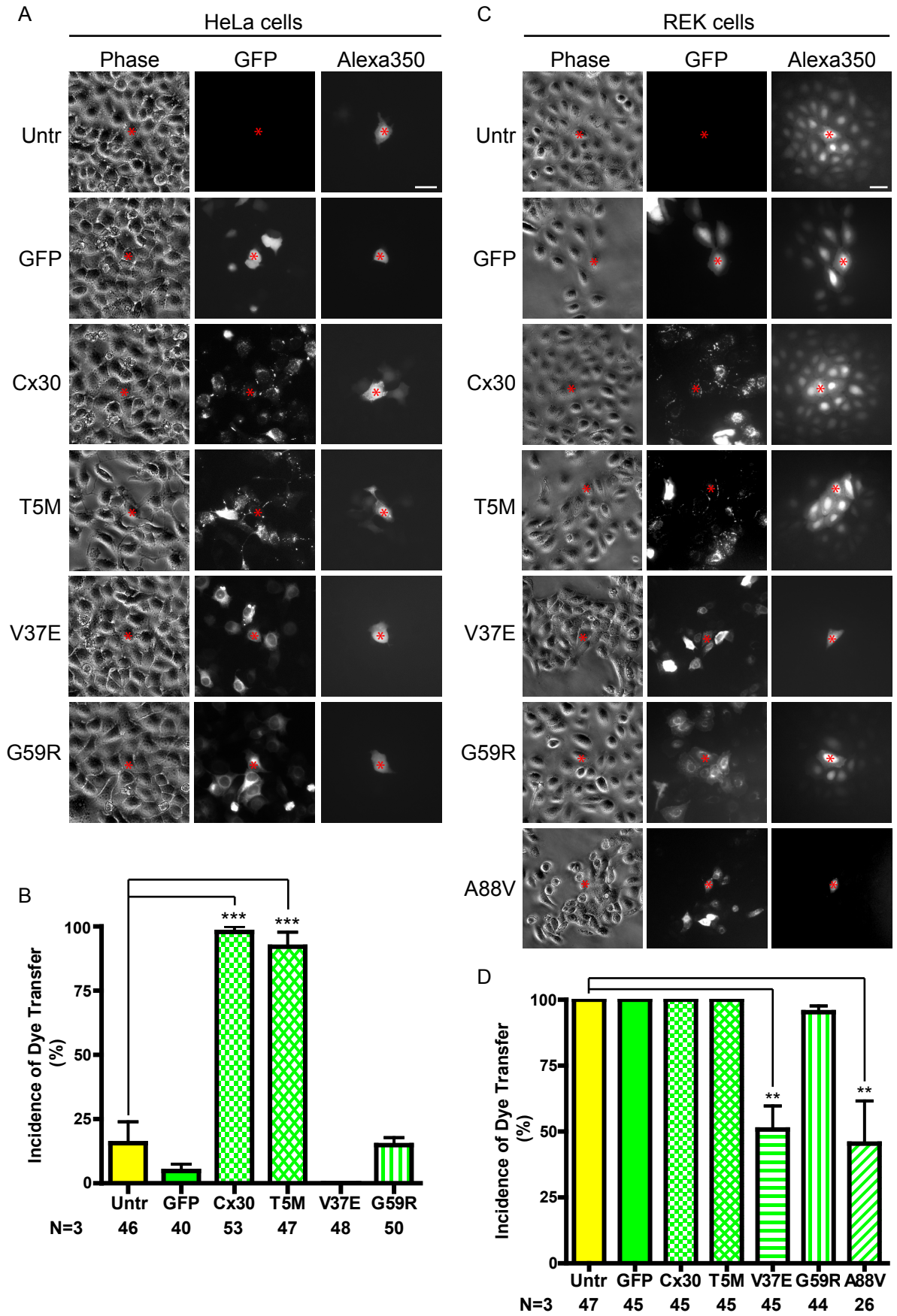
A
HeLa cells
Phase
GFP
Alexa350
Untr
GFP
Cx30
T5M
V37E
G59R
C
REK cells
Phase
GFP
Alexa350
Untr
GFP
Cx30
T5M
V37E
G59R
A88V
B
Incidence of Dye Transfer (%)
100
75
50
25
0
***
***
Untr GFP Cx30 T5M V37E G59R
N=3 46 40 53 47 48 50
D
Incidence of Dye Transfer (%)
100
75
50
25
0
**
**
Untr GFP Cx30 T5M V37E G59R A88V
N=3 47 45 45 45 45 44 26

FIGURE 4

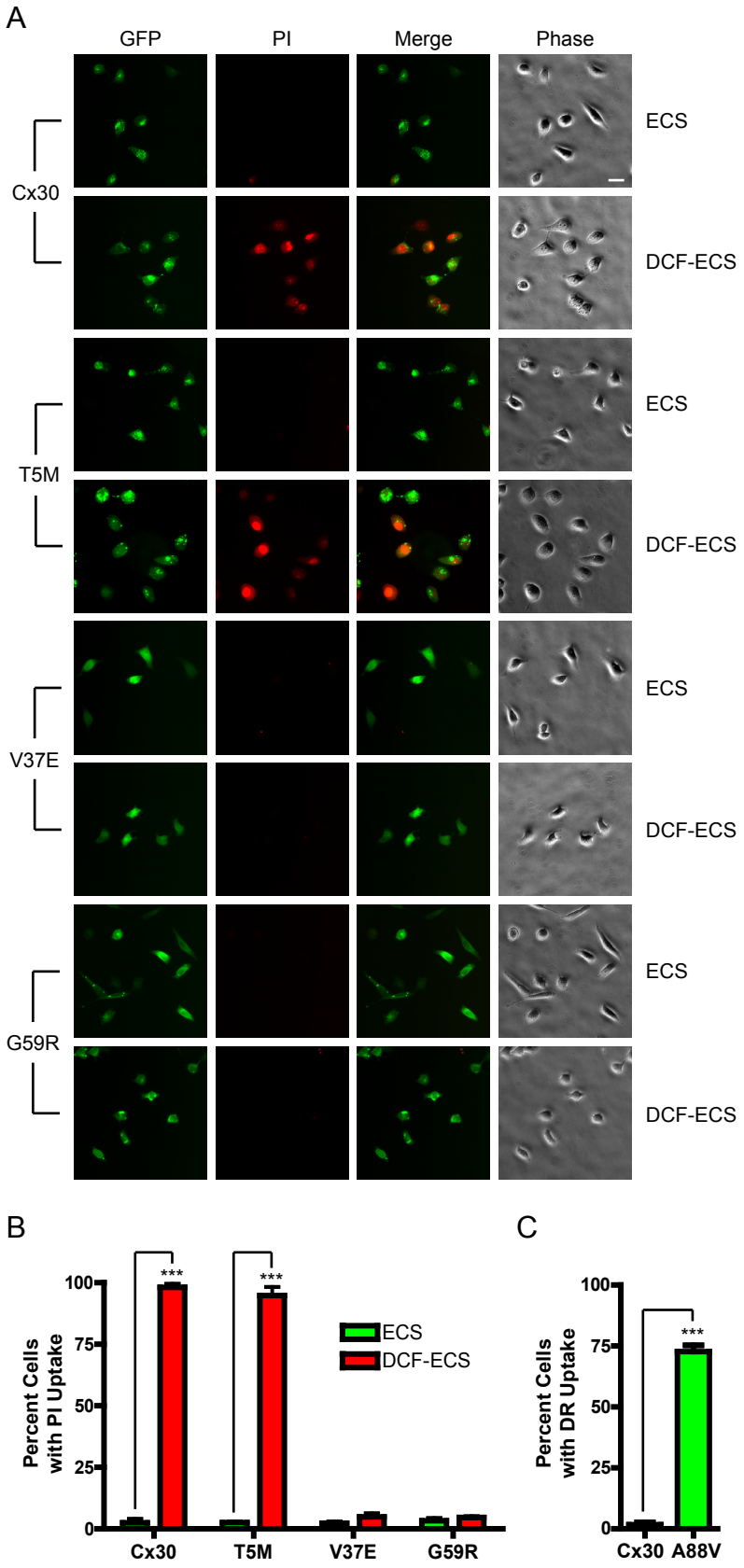
A
GFP
PI
Merge
Phase
Cx30
ECS
DCF-ECS
T5M
ECS
DCF-ECS
V37E
ECS
DCF-ECS
G59R
ECS
DCF-ECS
B
Percent Cells with PI Uptake
100
75
50
25
0
***
***
ECS
DCF-ECS
Cx30
T5M
V37E
G59R
C
Percent Cells with DR Uptake
100
75
50
25
0
***
Cx30
A88V

FIGURE 5

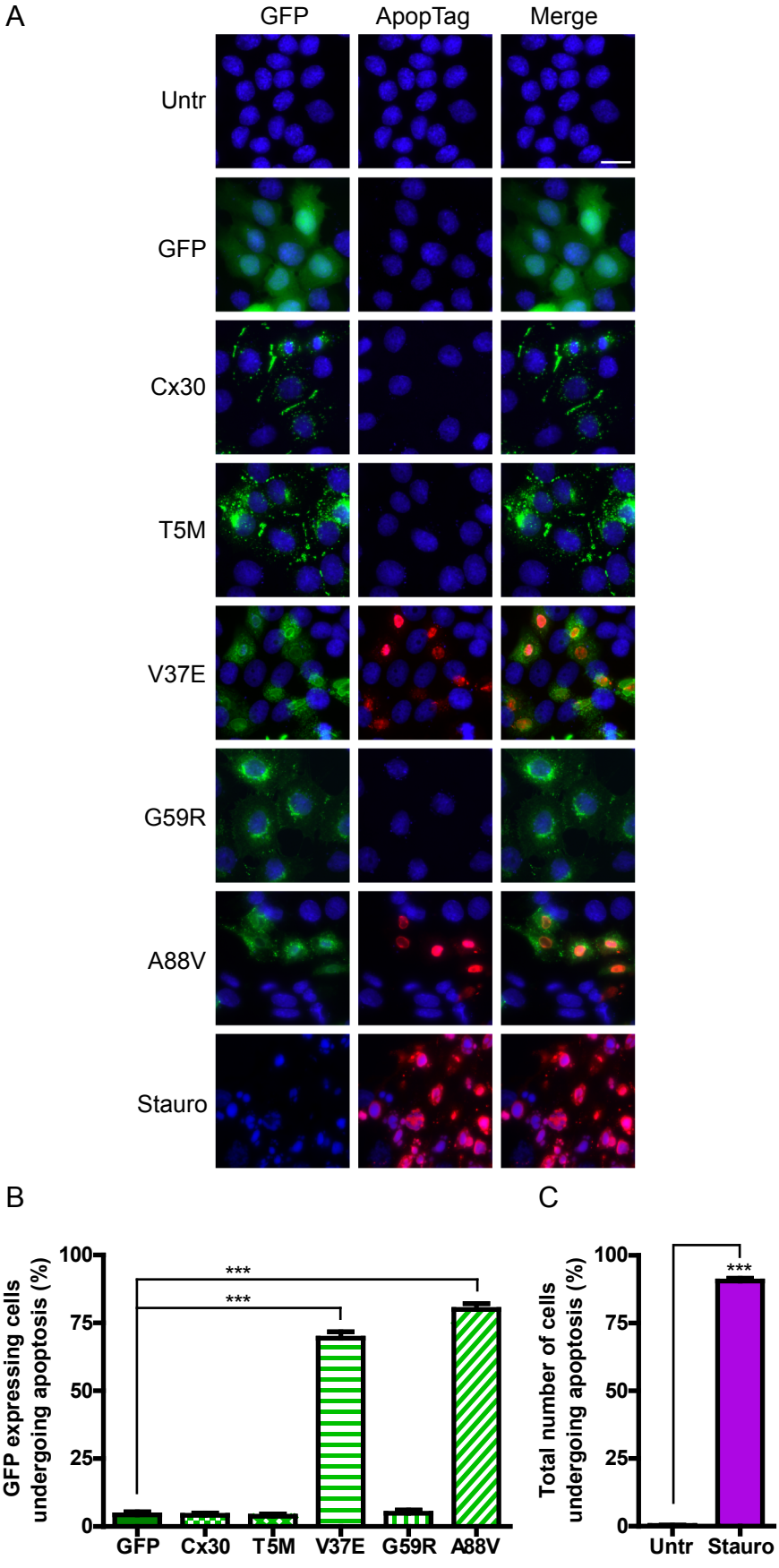
A
GFP
ApopTag
Merge
Untr
GFP
Cx30
T5M
V37E
G59R
A88V
Stauro
B
GFP expressing cells undergoing apoptosis (%)
100
75
50
25
0
***
***
GFP
Cx30
T5M
V37E
G59R
A88V
C
Total number of cells undergoing apoptosis (%)
100
75
50
25
0
***
Untr
Stauro

FIGURE 6

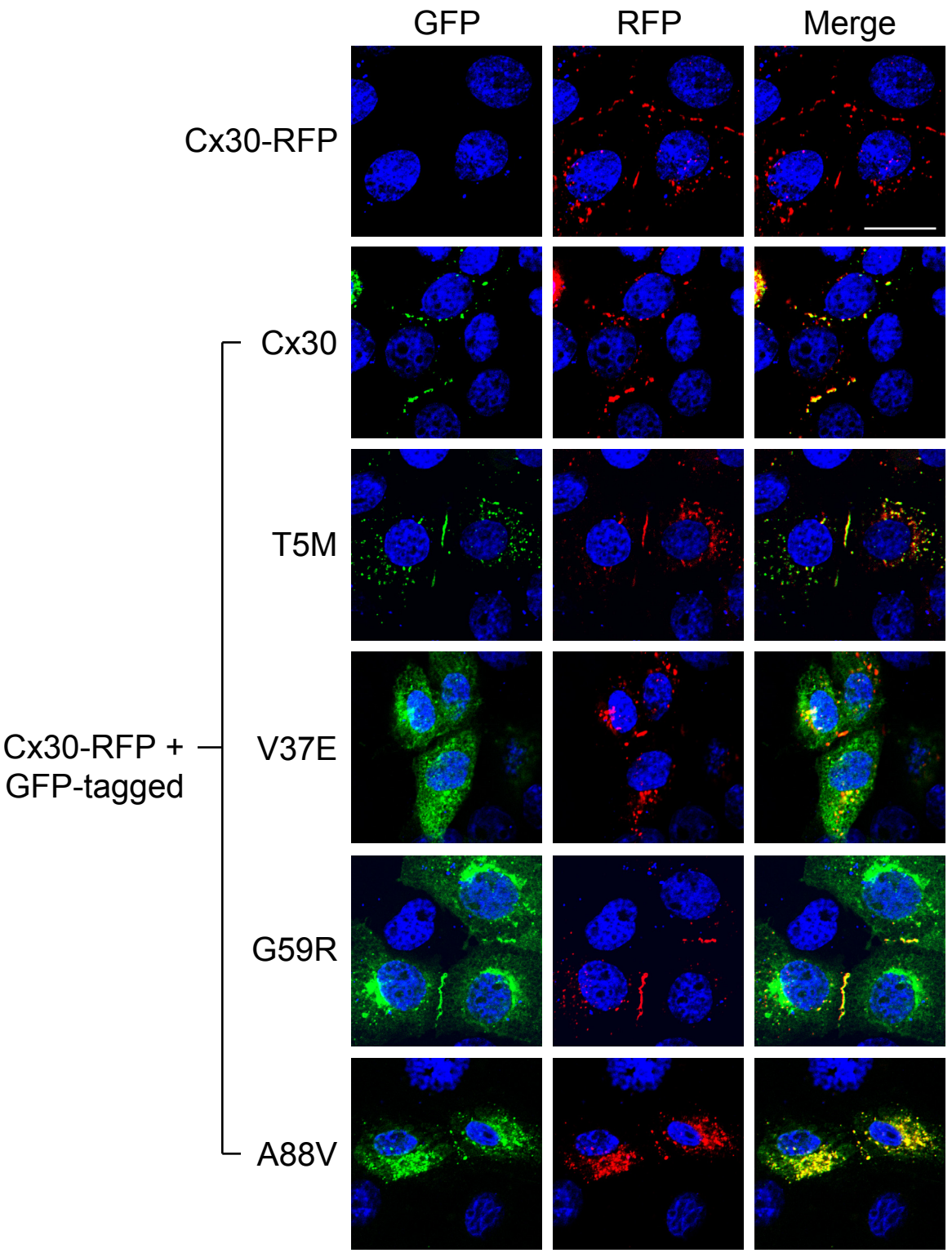
GFP
RFP
Merge
Cx30-RFP
Cx30-RFP +
GFP-tagged
Cx30
T5M
V37E
G59R
A88V

FIGURE 7

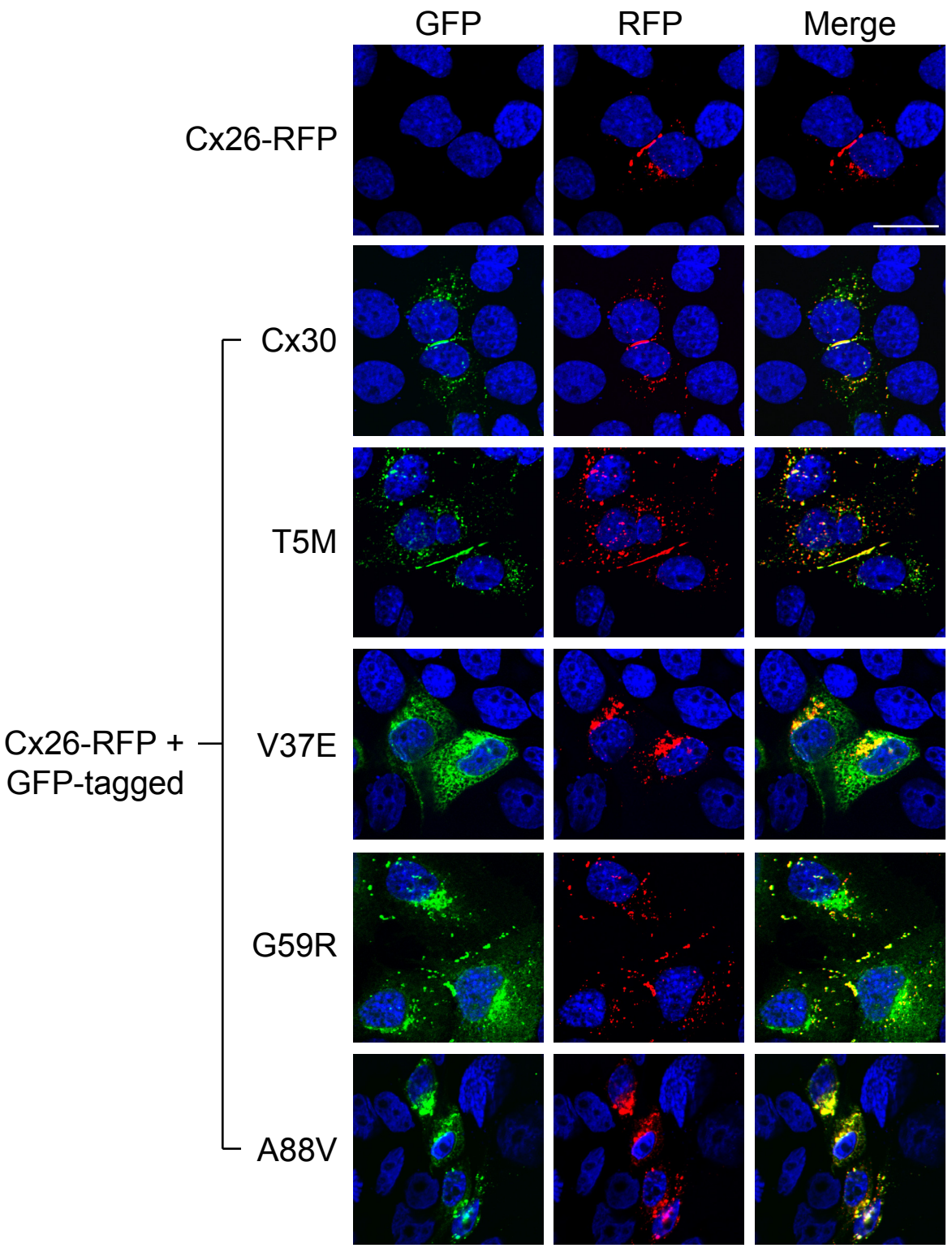
GFP
RFP
Merge
Cx26-RFP
Cx30
T5M
Cx26-RFP +
GFP-tagged
V37E
G59R
A88V

FIGURE 8

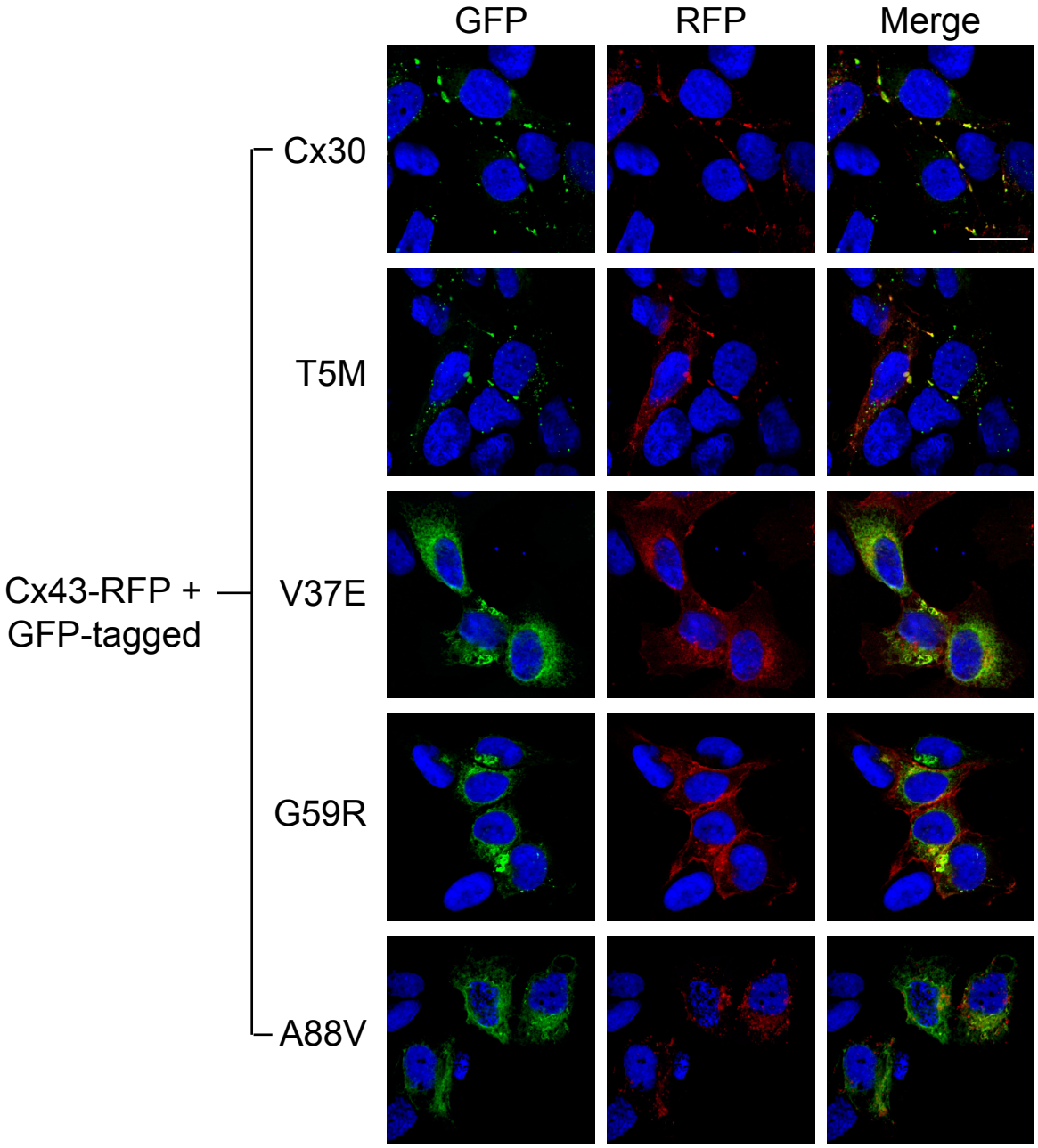

FIGURE S1

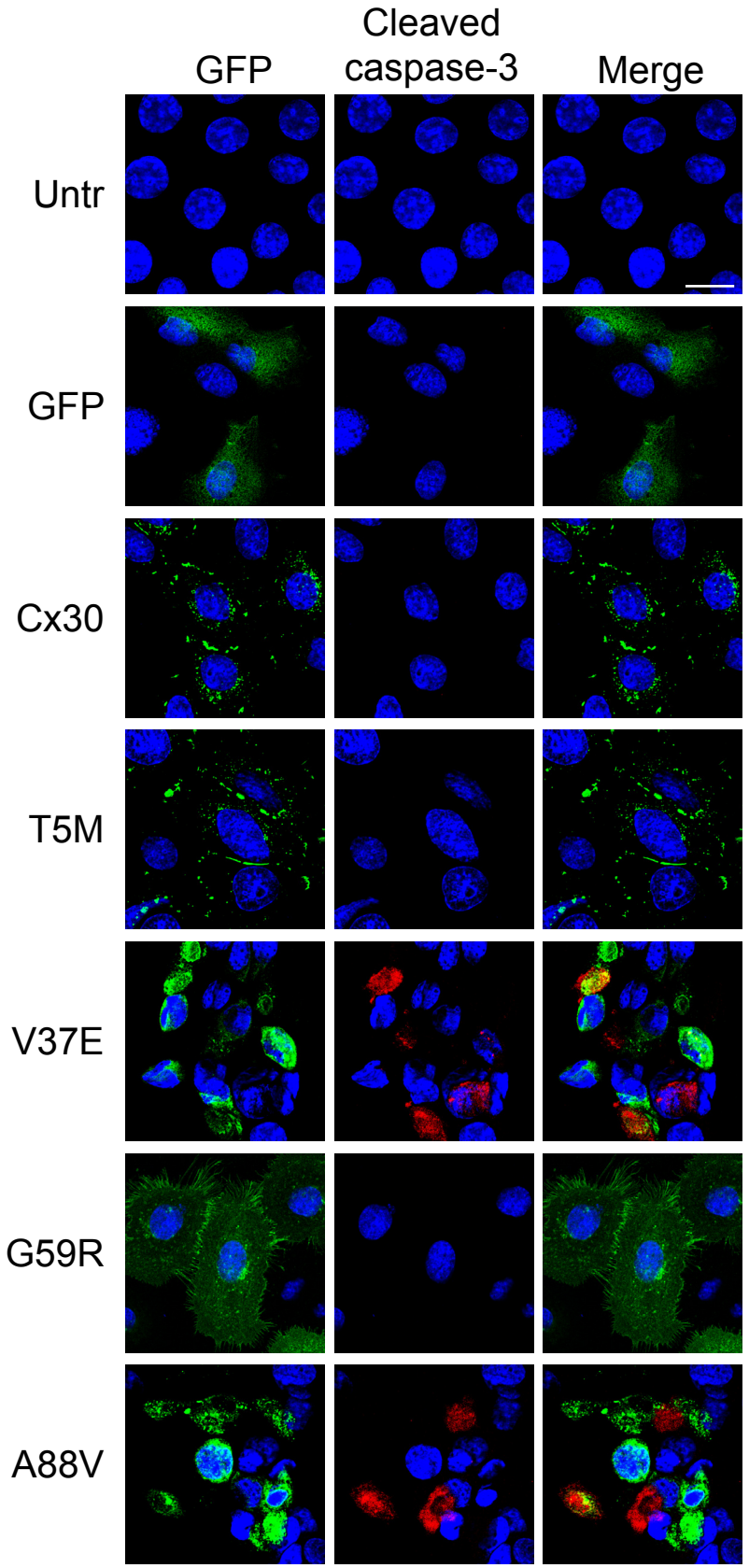

FIGURE S2

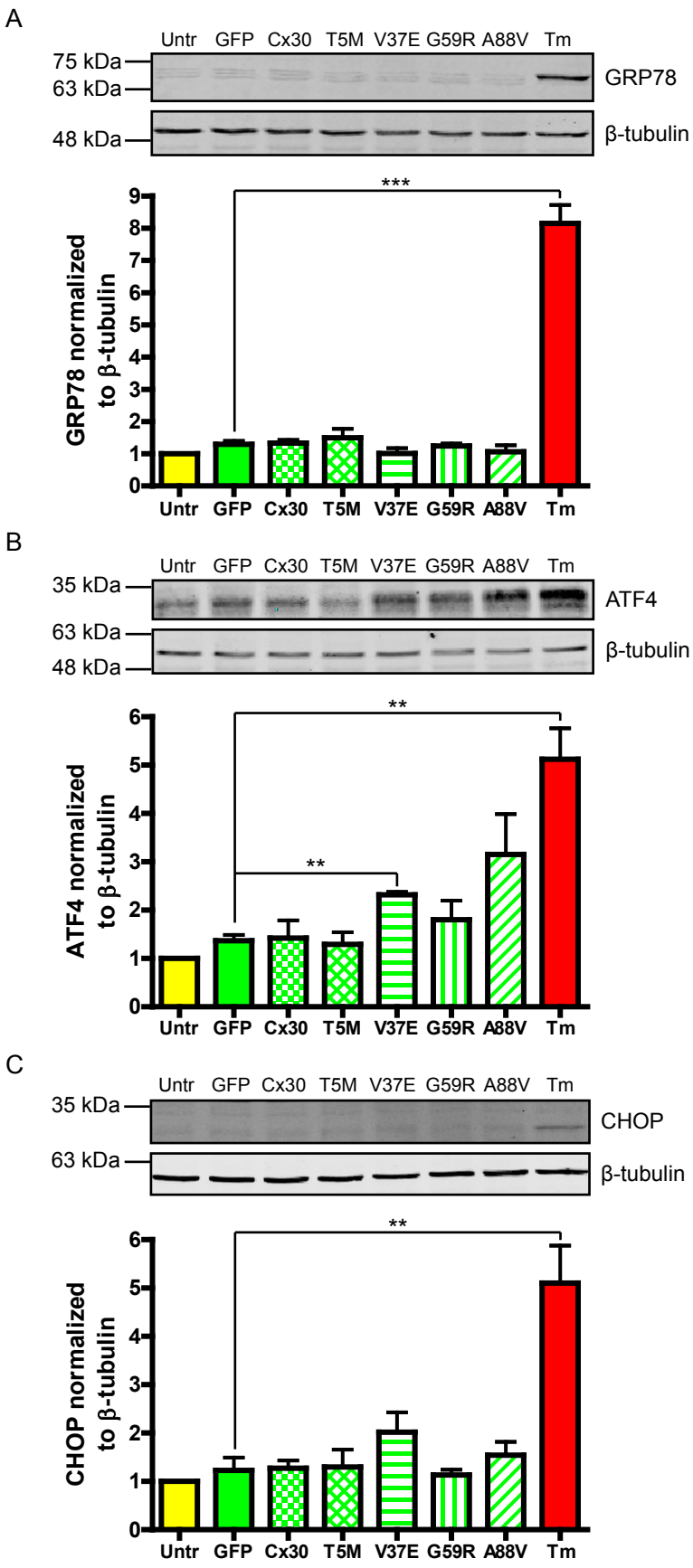
A
Untr GFP Cx30 T5M V37E G59R A88V Tm
75 kDa
63 kDa
GRP78
48 kDa
β-tubulin
***
GRP78 normalized to β-tubulin
0 1 2 3 4 5 6 7 8 9
Untr GFP Cx30 T5M V37E G59R A88V Tm
B
Untr GFP Cx30 T5M V37E G59R A88V Tm
35 kDa
ATF4
63 kDa
β-tubulin
48 kDa
**
**
ATF4 normalized to β-tubulin
0 1 2 3 4 5 6
Untr GFP Cx30 T5M V37E G59R A88V Tm
C
Untr GFP Cx30 T5M V37E G59R A88V Tm
35 kDa
CHOP
63 kDa
β-tubulin
**
CHOP normalized to β-tubulin
0 1 2 3 4 5 6
Untr GFP Cx30 T5M V37E G59R A88V Tm

FIGURE S3

A

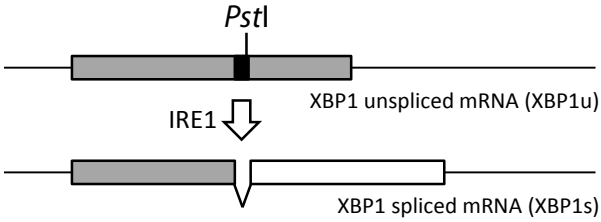

	Band sizes	*Pst*I digestion
Unspliced	601 bp	289 & 312 bp
Spliced	575 bp	575 bp

B

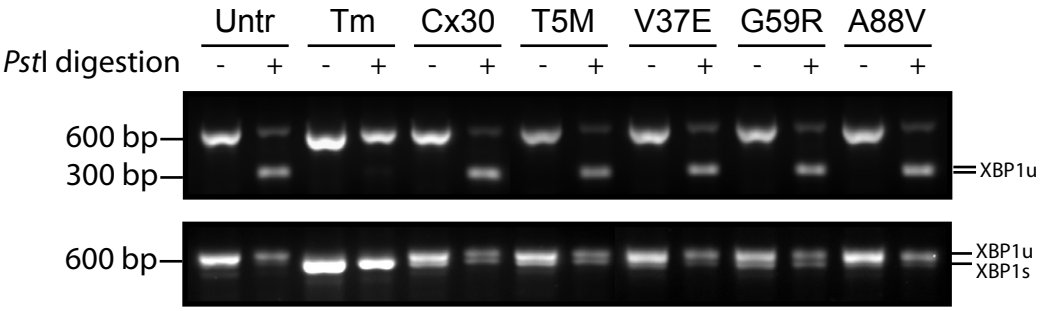

C

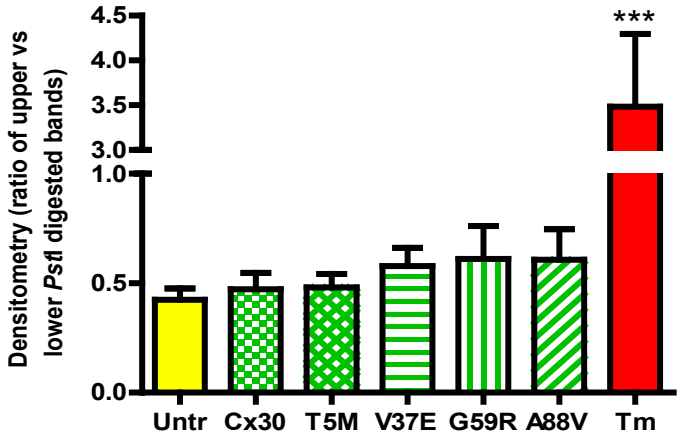

FIGURE S4

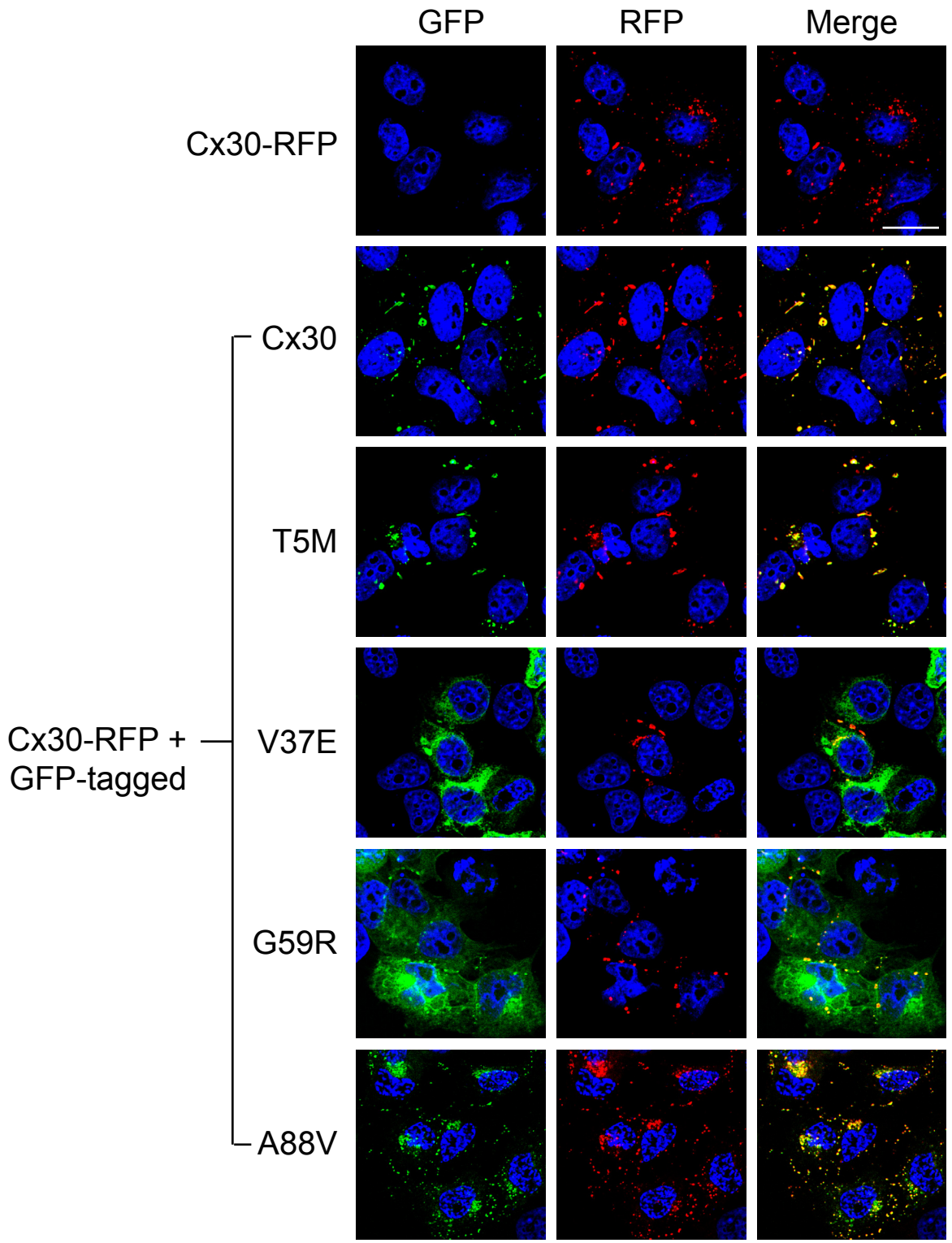
GFP
RFP
Merge
Cx30-RFP
Cx30-RFP +
GFP-tagged
Cx30
T5M
V37E
G59R
A88V

FIGURE S5

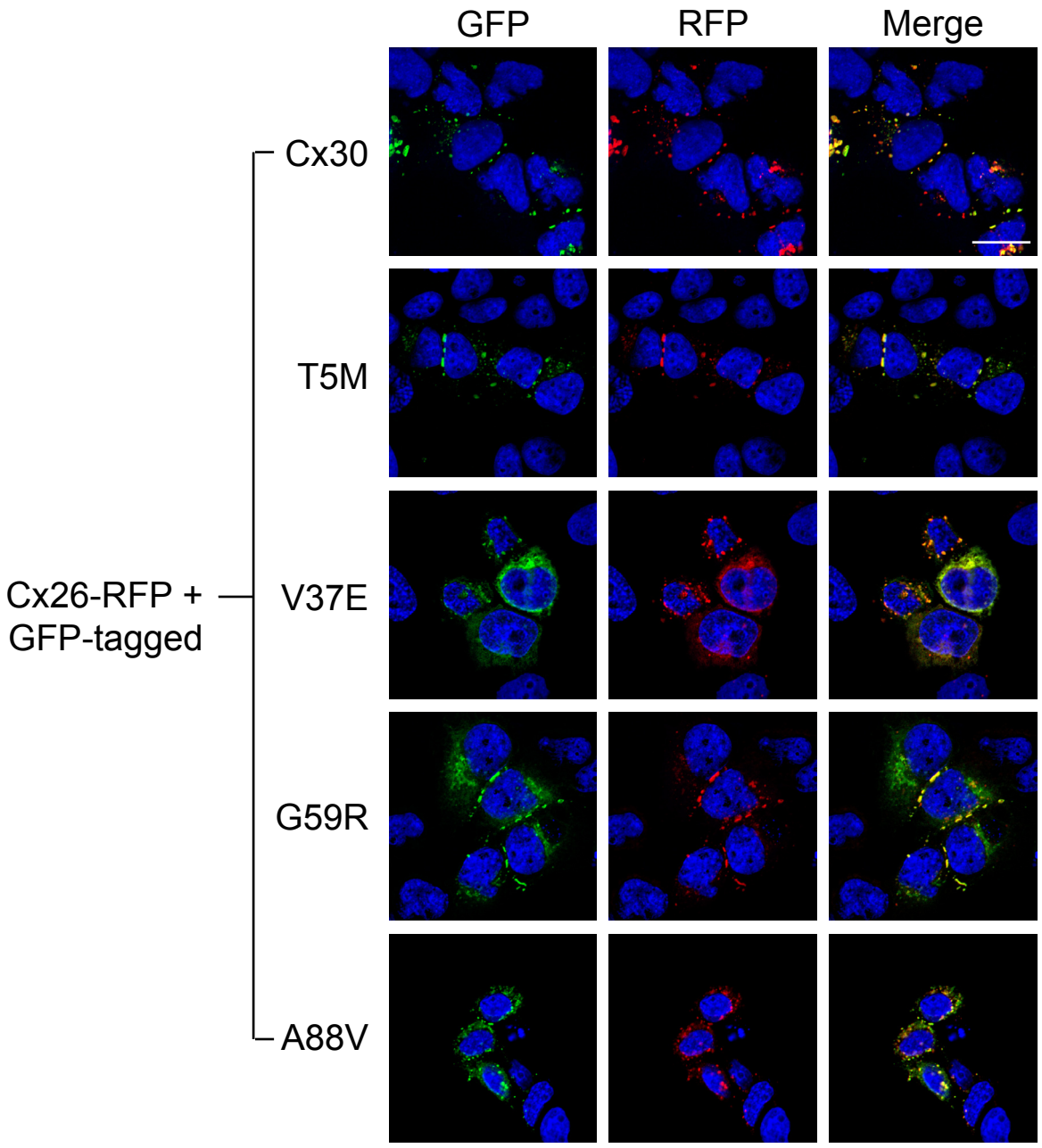

FIGURE S6

FOR REVIEWER'S ONLY

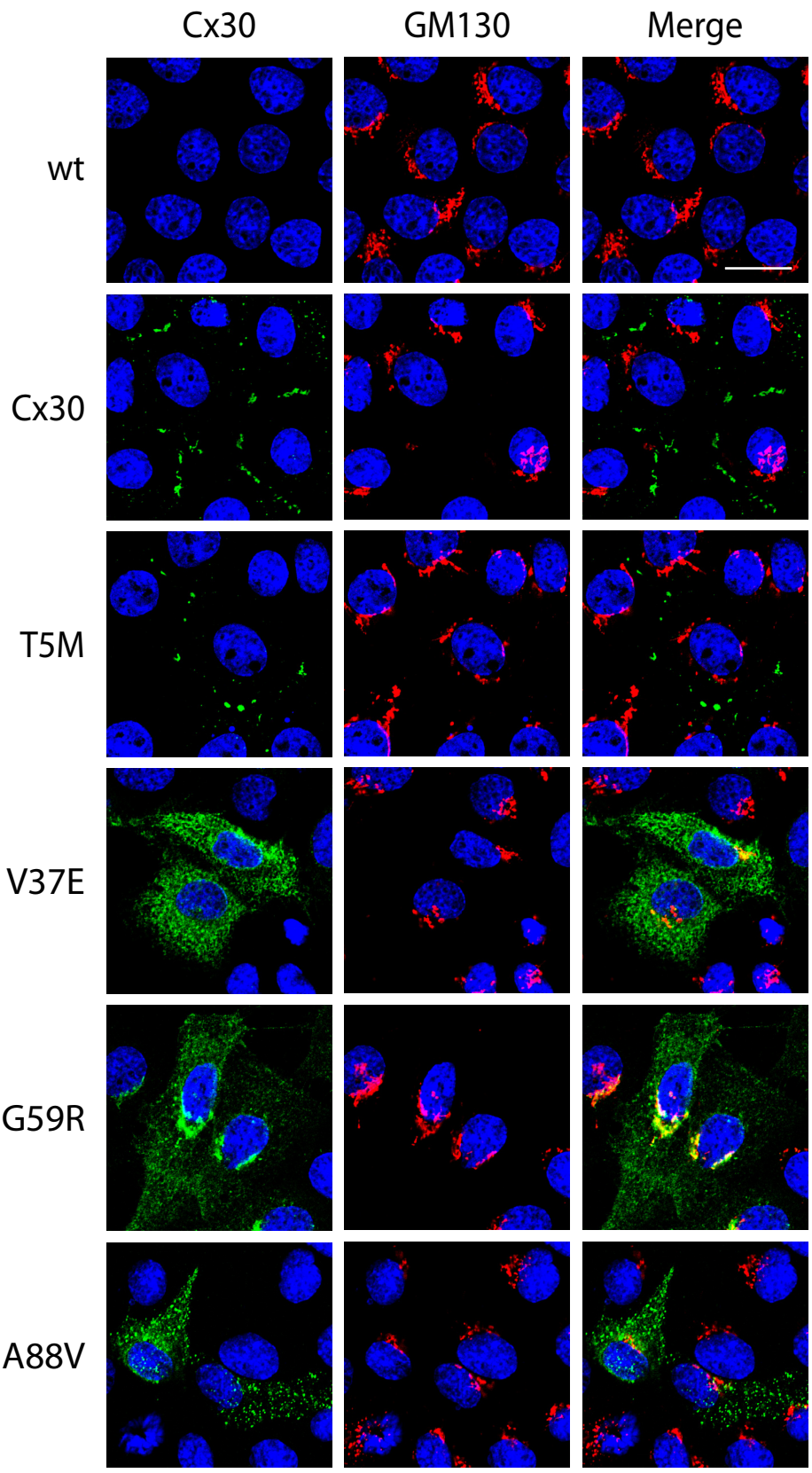

REV. FIG. 1

FOR REVIEWER'S ONLY

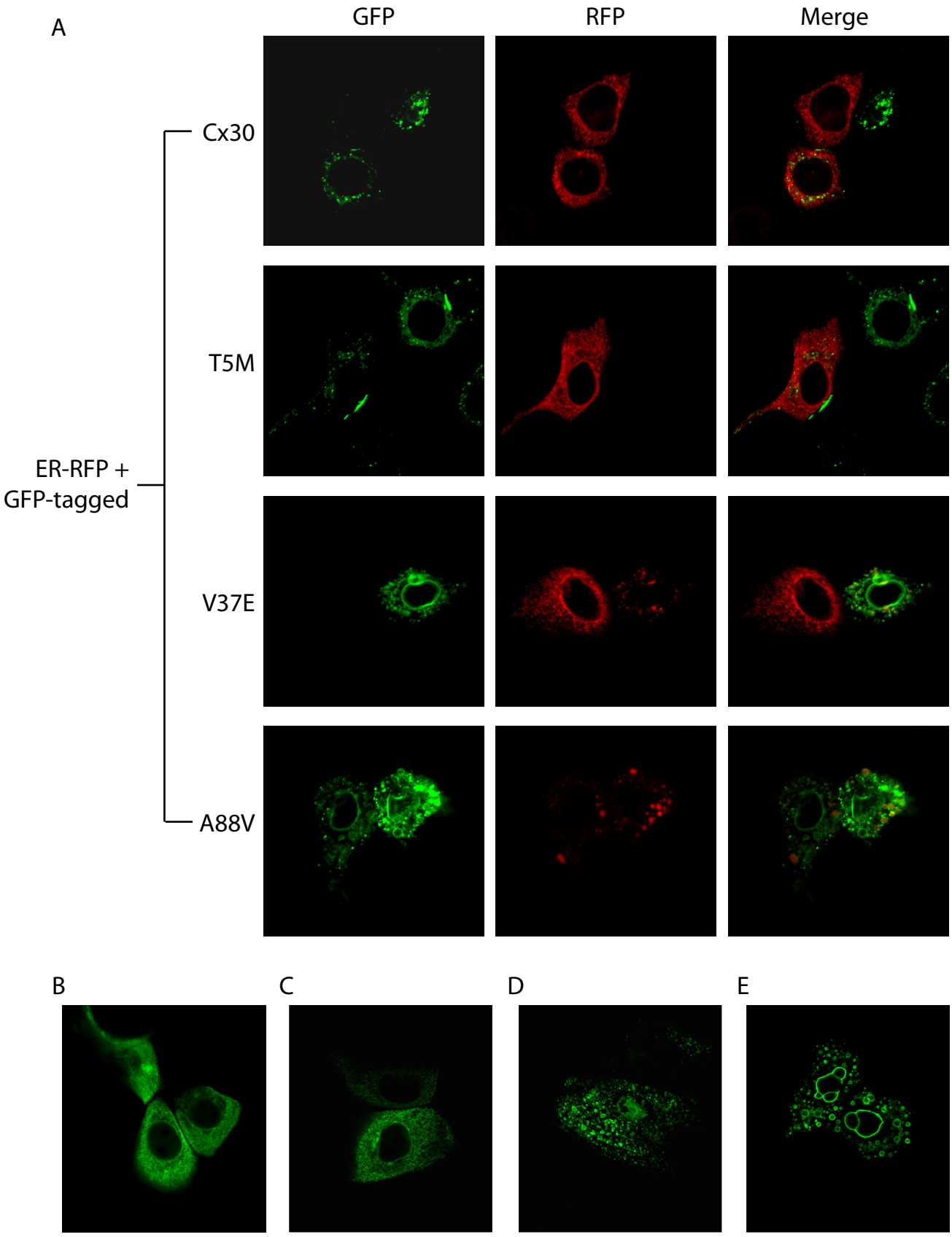

REV. FIG. 2